On the predictive capability and stability of rubber material models

by

Haining Zheng

B.E. Mechanical Engineering, Shanghai Jiao Tong University (2004)

Submitted to the School of Engineering

in partial fulfillment of the requirements for the degree of

Master of Science in Computation for Design and Optimization

at the

MASSACHUSETTS INSTITUTE OF TECHNOLOGY

September 2008

Author ……………………………………………………………………….…………….
School of Engineering
August 14, 2008

Certified by……………………………..…………………………………………..………...
Klaus-Jürgen Bathe
Professor of Mechanical Engineering
Thesis Supervisor

Accepted by…………………..…………………………………………………..…………..
Jaime Peraire
Professor of Aeronautics & Astronautics
Co-director, Computation for Design and Optimization

On the predictive capability and stability of rubber material models

by

Haining Zheng

Submitted to the School of Engineering
on August 14th, 2008, in partial fulfillment of the
requirements for the degree of
Master of Science in Computation for Design and Optimization

ABSTRACT

Due to the high non-linearity and incompressibility constraint of rubber materials, the predictive capability and stability of rubber material models require specific attention for practical engineering analysis.

In this thesis, the predictive capability of various rubber material models, namely the Mooney-Rivlin model, Arruda-Boyce model, Ogden model and the newly proposed Sussman-Bathe model, is investigated theoretically with continuum mechanics methods and tested numerically in various deformation situations using the finite element analysis software ADINA. In addition, a recently made available stability criterion of rubber material models is re-derived and verified through numerical experiments for the above four models with ADINA. Thereafter, the predictive capability and stability of material models are studied jointly for non-homogenous deformations.

The Mooney-Rivlin model, Arruda-Boyce model, Ogden model have difficulties in describing the uniaxial compression data while the Sussman-Bathe model can fit both compression and extension data well. Thus, the Sussman-Bathe model has the best predictive capability for pure shear deformations. Furthermore, with respect to more complex non-homogenous deformations, a conclusion is drawn that all three major deformations, namely uniaxial deformation, biaxial deformation and pure shear deformation, must satisfy the stability criterion to obtain physically correct non-homogenous simulation results.

Thesis supervisor: Klaus-Jürgen Bathe
Title: Professor of Mechanical Engineering

Acknowledgements

I would first like to thank my thesis advisor, Professor Klaus-Jürgen Bathe, for his support during my thesis work. I have had the most wonderful fortune of having him as my advisor. With his guidance and counsel, I learned the professional way of conducting research, especially on how to view a problem in a more physical and in-depth way. I believe strongly that this will benefit me tremendously in my future graduate study and my entire life. I am truly grateful for his insights and trust. Besides, I am thankful to ADINA R&D, Inc. for allowing me to use their proprietary software ADINA for my research work.

I am also very thankful to my lab colleagues: Jared, Christian, Jingzhong and Joris, especially I am grateful to Professor Tianyun Liu, Do-Nyun Kim and Reza Sharifi Sedeh for their invaluable help and encouraging attitude throughout my thesis research. I greatly appreciate the many helpful discussions and the interesting time spent together.

I must also acknowledge the friends I made during my time at MIT, especially the community of the CDO program: Professor Jaime Peraire, Professor Robert Freund, Laura Koller, Jocelyn Sales and my fellow classmates of the CDO program. Our friendships built during these 14 months will last for a lifetime. I would like to especially acknowledge my appreciation toward Alex Tan, who has always been taking care of me even before I joined MIT, and his great help in proof reading my thesis.

Finally, above all I want to express my gratitude to my parents and my girlfriend.

Their warm encouragement and love have always been the motivation of my progress although we are thousands of miles away and have not seen one another for 14 months. Without their strong support, I would never have been able to survive my most difficult time at MIT.

Contents

List of Figures

List of Tables

Chapter 1

Introduction

1.1 Motivation

Rubber materials, also referred as hyperelastic materials, are typically subjected to large deformations and they usually remain nearly incompressible[1]. Correspondingly, they have a relatively low elastic shear modulus and a high bulk modulus.

Rubber and rubber-like materials are widely used in different industries, in the established automotive and aerospace industries as well as in the rapidly emerging biomedical industry. For instance, various human soft tissues and artificial organs are hyperelastic in nature and can be modeled as rubber-like materials[2,3]. Also, hyperelasticity material models form the basis for more complex nonlinear material models, like elastoplasticity, viscoelasticity and viscoplasticity.

However, as the elasticity of a rubber material is highly nonlinear, accurately describing its mechanical property has always been a great challenge. Although various rubber material models have been proposed, they are mostly limited to a very small validity scope or are only valid for a certain type of deformation. Furthermore, due to rubber's incompressibility, rubber material models are often not stable, which induces great numerical difficulty when implemented numerically, for example using the finite element method.

Thus, a thorough study on the predictive capability and stability of rubber material models is very valuable.

1.2 Previous works

There are two main approaches in studying rubber materials: continuum mechanics and statistical mechanics. Both approaches generally derive the strain energy density as a function of strain or deformation tensors. The derivative of strain energy density with respect to a particular strain component determines the corresponding stress component. Thereafter, the established stress-strain relationship can be applied during the finite element analysis.

Among various rubber material models, the most commonly used models in practice are the Mooney-Rivlin model[4,5] and Ogden model[6], which are based on the phenomenological description of observed behavior as well as the Arruda-Boyce model[7] which is derived from arguments about the underlying structure of the rubber materials. In late 2007, Sussman and Bathe[8] proposed a new rubber material model based on the separability of strain energy density. The Sussman-Bathe model does not produce an explicit expression of the strain energy density but uses cubic splines to describe it. The model could attain high accuracy in predicting rubber material mechanical behavior and it is easy to implement numerically using the finite element method.

After these rubber material models were proposed, various researchers have studied and compared the predictive capability of the above models. Arruda and

Boyce[9] gave an excellent literature review of several important rubber material models. They first built material models using uniaxial extension data and then compared their pure shear deformation predictive capability. P.A.J. van den Bogert and R. de. Borst[10] also determined constants of different rubber material models through curve-fitting of uniaxial extension data and compared the performance of different material models undergoing non-homogenous deformations. Lastly, Przybylo and Arruda[11] used only compression experimental data to fit constants of the Arruda-Boyce model and got a comparably accurate response.

A proposed rubber material model with good predictive capability should be able to accurately describe the mechanical behavior of rubber. However, the stability of the proposed rubber material model is also required and is the key criterion in generating a physically and reasonable numerical result. Previous researchers mainly focused on the predictability of rubber material models and not much literature has addressed the stability issue. In addition, the structural stability and material stability are not clearly distinguished. Some researchers studied the stability problem mathematically[12] and employed the concept of Drucker stability[13] to study the stability with respect to the Green-Lagrange strain. However, in fact, the stability with respect to incremental displacements is more essential for finite element analysis[1].

1.3 Thesis scope

The main goal of this thesis is to determine the predictive capability and stability of the Mooney-Rivlin, Ogden, Arruda-Boyce and Sussman-Bathe models. The predictive capability and stability of these rubber material models are mathematically studied with continuum mechanics and further tested numerically using the finite element analysis software ADINA.

Both extension and compression data are necessary to obtain an accurate prediction[8]. Hence, rubber material models were built using both extension and compression experimental data simultaneously and thereafter their predictive capability for both pure shear and non-homogenous deformations is analyzed.

The stress-strain relationship is studied and its first derivative should be well-behaved[14]. A stability criterion with respect to incremental displacements is derived and tested numerically. Lastly, the results of the non-homogenous deformations are analyzed together with the stability of rubber material models.

1.4 Thesis outline

In chapter 2, the continuum mechanics theories and assumptions of the rubber material models are first reviewed, followed by the theoretical comparison of the advantages and constraints of different rubber material models. In chapter 3, the predictive capability for pure shear and non-homogenous deformations of various rubber material models is analyzed. In chapter 4, the stability criterion used in ADINA is re-derived, tested and employed to analyze the non-homogenous shear deformation test results. At the same time, improvements of the different rubber material models are suggested. Lastly, conclusions together with suggestions for future work are given in chapter 5.

Chapter 2

Rubber material models

As described in references[1, 9, 19, 34], the mechanical behavior of rubber materials can be presented by the strain energy density function, from which the stress-strain relationships can be derived.

2.1 Invariant based strain energy density function

Regarding the expression of strain energy density W, it should be quasi-convex and more likely poly-convex with respect to the deformation gradient X at its minimum[15, 16]. Furthermore, the strain energy density function of an isotropic hyperelastic material must satisfy the principles of frame indifference with respect to the tensor coordinates and thus is only a function of invariants of the right Cauchy-Green deformation tensor $C = X^T X$. Thus, generally, the strain energy density function W of an isotropic hyperelastic material can be expressed in polynomial terms of the invariants of the Right Cauchy-Green deformation tensor C:

$$W = W(C) = W(I_1, I_2, I_3) \tag{2.1}$$

where $\begin{cases} I_1 = tr(C) \\ I_2 = \dfrac{1}{2}(tr(C^2) - tr(C)^2) \\ I_3 = \det(C) \end{cases}$.

A typical invariant based rubber material model is the Mooney-Rivlin model[4] with the strain energy density function expressed as:

$$W(I_1, I_2) = C_1(I_1 - 3) + C_2(I_2 - 3) \tag{2.2}$$

where C_1 and C_2 are constants fitted from experimental data.

The Mooney-Rivlin model is simple and straight forward. However, experiments by Obata, Kawabata and Kawai[17] showed that C_1 and especially C_2 in fact vary with both I_1 and I_2 instead of staying constant. Further experiments demonstrated that the Mooney-Rivlin model only works well with rubber materials for strains up to 200%. Hence, Rivlin[5] enhanced the expression to

$$W = \sum_{i,j=0}^{\infty} C_{ij}(I_1 - 3)^i (I_2 - 3)^j \tag{2.3}$$

However, using higher order polynomials to fit experimental data can cause huge oscillations outside the experimental data range. Furthermore, there is hardly any physical meaning for the higher order constants.

2.2 Principal stretch based strain energy density function

When the deformation gradient X is expressed in the principal strain directions, the Right Cauchy-Green deformation tensor C can be expressed with its eigenvalues $\lambda_1^2, \lambda_2^2, \lambda_3^2$ and the invariants of the Right Cauchy-Green deformation tensor C are related in the following manner:

$$\begin{cases} I_1 = \lambda_1^2 + \lambda_2^2 + \lambda_3^2 \\ I_2 = \lambda_1^2\lambda_2^2 + \lambda_2^2\lambda_3^2 + \lambda_3^2\lambda_1^2 \\ I_3 = \lambda_1^2\lambda_2^2\lambda_3^2 \end{cases} \tag{2.4}$$

Therefore, the expression of total strain energy density function can be expressed in terms of $\lambda_1^2, \lambda_2^2, \lambda_3^2$

$$W = W(I_1, I_2, I_3) = W(\lambda_1^2, \lambda_2^2, \lambda_3^2) \tag{2.5}$$

However, Ogden questioned the necessity of restricting the form of the strain energy density function W to even-power functions of the extension ratio λ, as embodied in Rivlin's representation using the strain invariants. From the mathematical standpoint, it is also reasonable to use $\lambda_1^2, \lambda_2^2, \lambda_3^2$ instead of $\lambda_1, \lambda_2, \lambda_3$. Assuming separability of the strain energy density expression[18], Ogden expanded the polynomial expressions of the principal stretches $\lambda_1, \lambda_2, \lambda_3$ and proposed the Ogden model[6], whose strain energy density function is:

$$W(\lambda_1, \lambda_2, \lambda_3) = \sum_{p=1}^{N} \frac{\mu_p}{\alpha_p}(\lambda_1^{\alpha_p} + \lambda_2^{\alpha_p} + \lambda_3^{-\alpha_p} - 3) \tag{2.6}$$

For particular values of material constants $(N = 2, \alpha_1 = 2, \alpha_2 = -2)$, the Ogden model reduces to the Mooney-Rivlin material.

The Ogden model works well for incompressible rubber materials for strains up to very large values. It captures the state of rubber material deformations for the entire stretching range, except near the limiting stretch region.

However, to fit the experimental data curve, the Ogden model normally requires at least six parameters completely devoid of any physical insight into the mechanics governing that state of deformation. Furthermore, similar to Rivlin's formula, huge oscillations outside the experimental data range may be experienced if the Ogden model is employed. In addition, another disadvantage of the Ogden model, in fact of any hyperelastic rubber material model expressed in principal stretch directions, is the difficulty in properly implementing the model in a general three-dimensional context.

Difficulties arise when two or more principal stretch directions become equal, where the denominator of the derivatives of the principal stretch direction with respect to the invariants becomes zero[10].

2.3 Statistical mechanics based strain energy density function

Using statistical mechanics is another approach to derive the strain energy density function. Instead of treating the rubber material as an assembly of particles, the statistical mechanics approach assumes that rubber material is a structure of randomly-oriented long molecular chains[19].

(a) Gaussian treatment

For small deformation, Gaussian treatment[20,21] is employed and the distribution of the end-to-end length r of a molecular chain is given by

$$P(r) = 4\pi(\frac{3}{2\pi nl^2})^{\frac{3}{2}} r^2 \exp(-\frac{3r^2}{2nl^2}) \quad (2.7)$$

where n is the number of links in the chain and l is the length of each link. Assuming that the chain length r does not approach its fully extended length nl, the strain energy density function W can be derived from the change in configurational entropy,

$$W_G = \frac{1}{2} NK\theta(\lambda_1^2 + \lambda_2^2 + \lambda_3^2 - 3) \quad (2.8)$$

where k is the Boltzmann's constant and θ is the absolute temperature.

(b) non-Gaussian statistical treatment

For large deformations, the non-Gaussian statistical effect must be considered and

Langevin chain statistics was employed to derive the force-extension relationship for a chain[9]:

$$f = \frac{k\theta}{l} L^{-1}(\frac{r}{nl}) = \frac{k\theta}{l} L^{-1}(\frac{\lambda}{\sqrt{n}}) \tag{2.9}$$

where $\frac{r}{nl} = \coth \beta - \frac{1}{\beta} = L(\beta)$.

To relate the above individual chain stretching with the whole body deformation, different network models such as the three chain model[22], four chain model[23, 24], full chain model[25] and eight chain model[7] were proposed. Each network model results in a different strain energy density function.

The Arruda-Boyce model[7], a non-Gaussian eight-chain molecular network model as shown in figure 2.1, is the most successful statistical mechanics model so far. The chains are located along the diagonals of the unit cell and deform with the cell. The interior junction point remains centrally located throughout the deformation and the stretching on each chain in the model is found to be the root mean-square of the applied stretching.

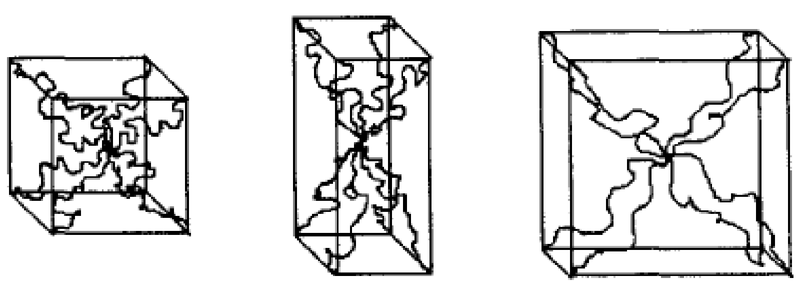

Figure 2.1 Eight-chain network model in its undeformed (left), uniaxial tension (center), and biaxial extension state (right) [7]

The strain energy density function W of the Arruda-Boyce model is derived as

$$W_{8ch} = \frac{Nk\theta}{2}\left[\beta_{chain}\lambda_{chain} + \sqrt{n}\ln(\frac{\beta_{chain}}{\sinh \beta_{chain}}) \right] \tag{2.10}$$

where $\begin{cases} \lambda_{chain} = (\frac{1}{3} I_1)^{\frac{1}{2}}; \\ \beta_{chain} = L^{-1}\left(\frac{\lambda_{chain}}{\sqrt{n}}\right). \end{cases}$

To implement the above formula in numerical analysis, the above function of strain energy density is converted into polynomial form as:

$$W_{8ch} = \mu \sum_{i=1}^{n} [\frac{C_i}{\lambda_m^{2i-2}} (I_1^i - 3^i)] \qquad (2.11)$$

Practically, the fifth order approximation of the expression is accurate enough,

$$W_{8ch} = \mu \sum_{i=1}^{5} [\frac{C_i}{\lambda_m^{2i-2}} (I_1^i - 3^i)] \qquad (2.12)$$

$$C_1 = \frac{1}{2}, C_2 = \frac{1}{20}, C_3 = \frac{11}{1050}, C_4 = \frac{19}{7050}, C_5 = \frac{519}{673750}$$

where μ is the initial shear modulus and λ_m is the locking stretch.

The experiment by Arruda and Boyce proved that this model is well suited for rubber materials such as silicon and neoprene with strain up to 300%. Furthermore, this model has no issue with curve-fitting even when the test data are limited[7.9].

One constraint of the Arruda-Boyce model is that in the small deformation range, it does not accord well with experimental data and needs to be combined with the Flory-Erman model[9]. Furthermore, the Arruda-Boyce model assumes a particular microscopic structure of rubber material. Hence, it only works well for rubber materials that have the corresponding microscopic structure. Some researchers[26] found that some rubber materials do not fit that particular microscopic structure assumption and hence the model does not work very well with such rubber materials.

2.4 Sussman-Bathe model

Sussman and Bathe[8] utilized the assumption that the strain energy density function W is a sum of separable strain energy density functions w and employed the true strain e instead of the principal stretch λ to express the total strain energy density function W.

First, cubic splines are employed to fit the uniaxial stress-strain curve and thus stress τ could be expressed as a function of true strain e. Subsequently, the relation between stress τ and the first derivative of the strain energy density function w' for uniaxial deformation

$$w'(e) = \sum_{k=0}^{\infty}[\tau((\frac{1}{4})^k e) + \tau(-\frac{1}{2}(\frac{1}{4})^k e)] \tag{2.13}$$

is utilized to express w' in terms of the true strain e. Thereafter, the first derivatives of the strain energy density function w' could be simply integrated to get the values of the strain energy density function w and the strain energy density function W expressed as

$$W = \sum_{i=1}^{3} w(e_i) \tag{2.14}$$

At last, instead of proposing an explicit analytical expression, uniform cubic splines are employed to calculate the values of the strain energy density function W.

No material constants need to be fitted for Sussman-Bathe model. In addition, given correct and enough experimental data, it can produce very accurate 3D simulation results. On the other hand, one constraint of the Sussman-Bathe model is that the uniaxial tension and compression data must be supplied and the compression data is typically obtained from the biaxial tension data. Another restriction is that the separability of strain energy density function W which the model is built on (like the original Mooney-Rivlin and Ogden models) must be applicable. However, this restriction may not hold when the strain gets very large[27]. Similar to other models, the accuracy of this model relies on the accuracy of experimental data; if the test data have been obtained over a sufficient large range of strain values, the Sussman-Bathe model will be able to represent the behavior of the rubber material well. However, if only limited data or even error data is supplied, the model may become both inaccurate and unstable.

2.5 Effects of compressibility

In the above four rubber material models, the deformations are assumed to be isometric. However in reality, rubber material is not completely incompressible under large strain. Meanwhile, to avoid numerical difficulties in finite element procedures[1], rubber materials are more readily implemented as nearly incompressible materials: a small measure of volumetric deformation is incorporated[28].

The total strain energy density function W can be decomposed into the deviatoric strain energy density W_D and the volumetric strain energy density W_V. To get the deviatoric strain energy density W_D, the volumetric part should be factored out. If $\widehat{C} = I_3^{-1/3} C$ is employed as new purely deviatoric Right Cauchy-Green deformation tensor, then

$$\frac{V}{V_0} = \det(\widehat{C}) = \det(I_3^{-1/3}C) = I_3^{-1}\det(C) = 1 \tag{2.15}$$

which means no change in volume, thus the volumetric part of C is eliminated . The deviatoric strain energy density W_D becomes

$$W_D = \widehat{W}_D(C) = W_D(\widehat{C}) = W_D(I_3^{-1/3}C) \tag{2.16}$$

Correspondingly, the invariants of tensor $\widehat{C}$ become

$$\begin{cases} I_1(I_3^{-1/3}C) = I_3^{-1/3}I_1 = J_1 \\ I_2(I_3^{-1/3}C) = I_3^{-2/3}I_2 = J_2 \\ I_3(I_3^{-1/3}C) = 1 \end{cases} \tag{2.17}$$

Hence to obtain the expression for the deviatoric strain energy density $\widehat{W}_D$, I_1, I_2 need to be substituted by new invariants J_1, J_2 in the original strain energy density function W_D and the corresponding expression is:

$$\widehat{W}_D = W_D(J_1, J_2) \tag{2.18}$$

which coincides with the procedure in ADINA[29]. For example, the deviatoric strain energy density function of the Mooney-Rivlin model is expressed as

$$W_D = C_1(J_1 - 3) + C_2(J_2 - 3) \tag{2.19}$$

Meanwhile, with κ as the bulk modulus, the expressions for volumetric strain energy density W_V are[29]:

$$W_v = \frac{1}{2}\kappa(J-1)^2 \text{ for Mooney-Rivlin model and Ogden model;} \tag{2.20}$$

$$W_v = \frac{\kappa}{2}\left[\frac{(J-1)^2}{2} - lnJ\right] \text{ for Arruda-Boyce model} \tag{2.21}$$

$$W_v = \kappa[JlnJ - (J-1)] \text{ for Sussman-Bathe model.} \tag{2.22}$$

Chapter 3

Predictive capability of material models

3.1 Pure shear deformation predictive capability analysis

3.1.1 Model building with Treloar's data in ADINA

(a). Experimental data from Treloar

Treloar's experimental data[30] of 8% sulphur rubber material at a temperature of 20^{o}C, shown in figure 3.1, has been intensively used in the analysis of rubber-like materials.

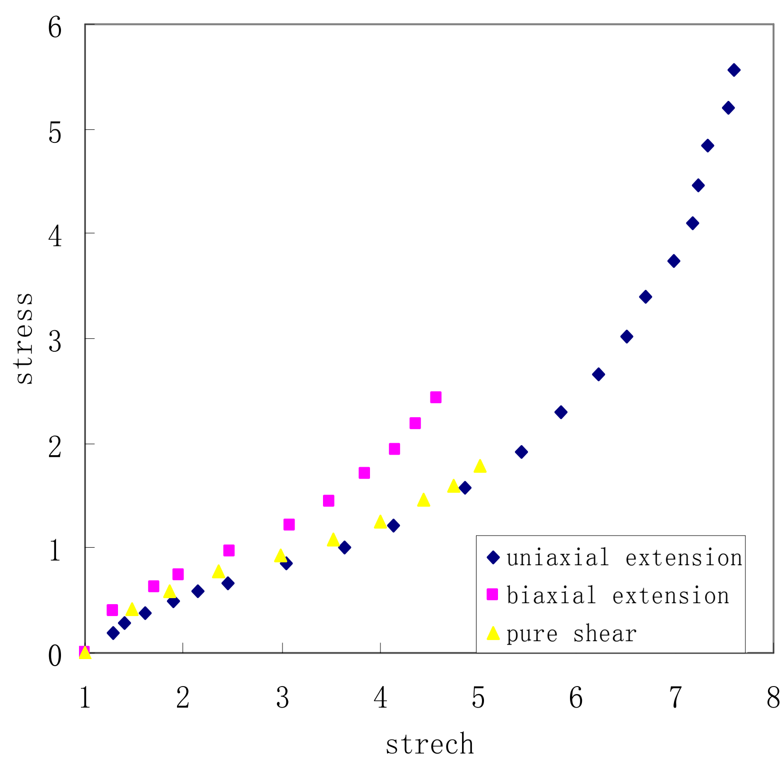

Figure 3.1 Treloar experimental data

As discussed in Sussman and Bathe's paper[31], the uniaxial compression experimental data is required to build a reasonable model. Due to the lack of original uniaxial compression data, the biaxial extension data is converted into uniaxial compression data as they are equivalent in nature[32]. Let the rubber materials be fully incompressible, and the conversion formulas are

$$\begin{cases} e_u = -2e_b,\ \lambda_{\mathrm{u}} = \lambda_b^{-2},\ {}_0\mathrm{e}_{\mathrm{u}} = (1+{}_0\mathrm{e}_{\mathrm{b}})^{-2} - 1 \\ \tau_{\mathrm{u}} = -\tau_{\mathrm{b}},\ {}_0\sigma_u = -\ {}_0\sigma_b \lambda_b^3 \end{cases} \tag{3.1}$$

where e_u is the equivalent uniaxial true strain (<0), e_b is the equibiaxial true strain (>0), λ_u is the equivalent uniaxial stretch, λ_b is the equibiaxial stretch, ${}_0\mathrm{e}_{\mathrm{u}}$ is the equivalent uniaxial engineering strain, ${}_0\mathrm{e}_{\mathrm{b}}$ is the equibiaxial engineering strain, τ_{u} is the equivalent uniaxial true stress, τ_{b} is the equibiaxial true stress, ${}_0\sigma_u$ is the equivalent engineering stress, ${}_0\sigma_b$ is the equibiaxial engineering stress.

The converted uniaxial compression data combined with given extension data is shown in table 3.1 and figure 3.2.

Table 3.1 Compression-extension experimental data from Treloar[27]

Engineering strain	Engineering stress
-0.95208	-231.306
-0.94772	-182.065
-0.94206	-139.154
-0.93266	-97.6023
-0.9178	-61.5612
-0.89524	-35.8418
-0.83626	-14.5029
-0.73935	-5.63367
-0.65665	-3.12989
-0.40084	-0.83984
0	0
0.2887	0.1966
0.4064	0.2835
0.6097	0.3795
0.8945	0.4851
1.1549	0.5955
1.448	0.6626
2.0502	0.8593
2.6364	1.0078
3.1326	1.2191
3.8647	1.5696
4.4419	1.9251
4.8317	2.2904
5.2214	2.6509
5.5052	3.0212
5.6994	3.3915
5.9914	3.7377
6.1857	4.0936
6.2331	4.4641
6.3377	4.8393
6.5318	5.2048
6.5957	5.5705

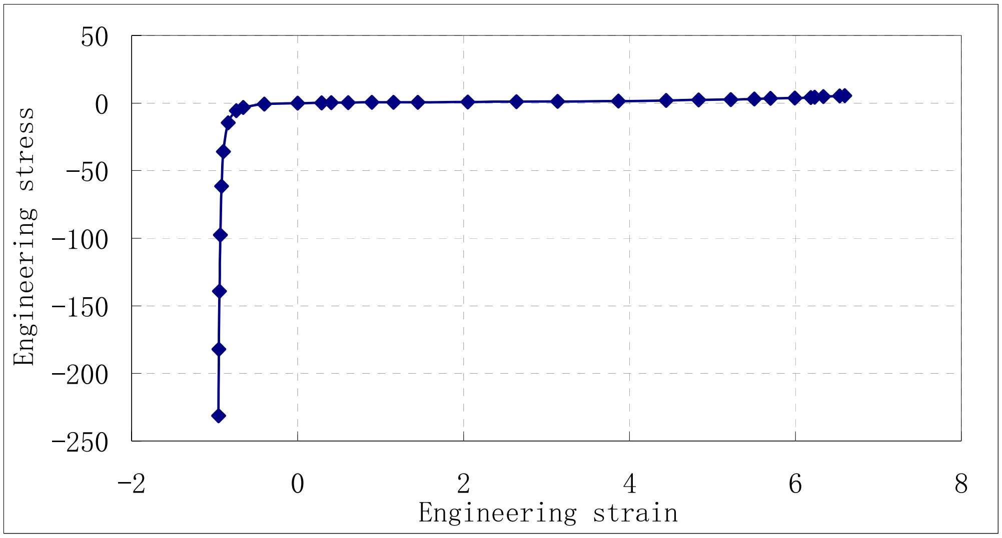

Figure 3.2 Extension and compression uniaxial data from Treloar[27]

(b). Constitutive relation curve fitting with Treloar data

As seen from the strain energy density functions of various rubber material models introduced in chapter 2, each model requires many constants from curve-fitting (except the Sussman-Bathe model). ADINA has a corresponding user interface to fit the experimental data and obtain these constants. Within ADINA user interface, there are two adjustable parameters for curve fitting. One parameter is the "Least square solution method", which has two options: Singular value decomposition (SVD) and Gaussian Elimination (GE). The other parameter is "Approximation order", ranging from 1 to 9. With different parameter settings, various curve-fitting results can be achieved and thereafter the most appropriate parameters for each material model can be chosen.

(i) Mooney-Rivlin model

The best fitted curve for the Mooney-Rivlin model is obtained using GE as the "Least square solution method" together with the order 3 approximation. Order 9 approximation produces similar result, but high order curves usually are more unstable, especially for the range beyond the experimental data. The constants of this model are shown in figure 3.3.

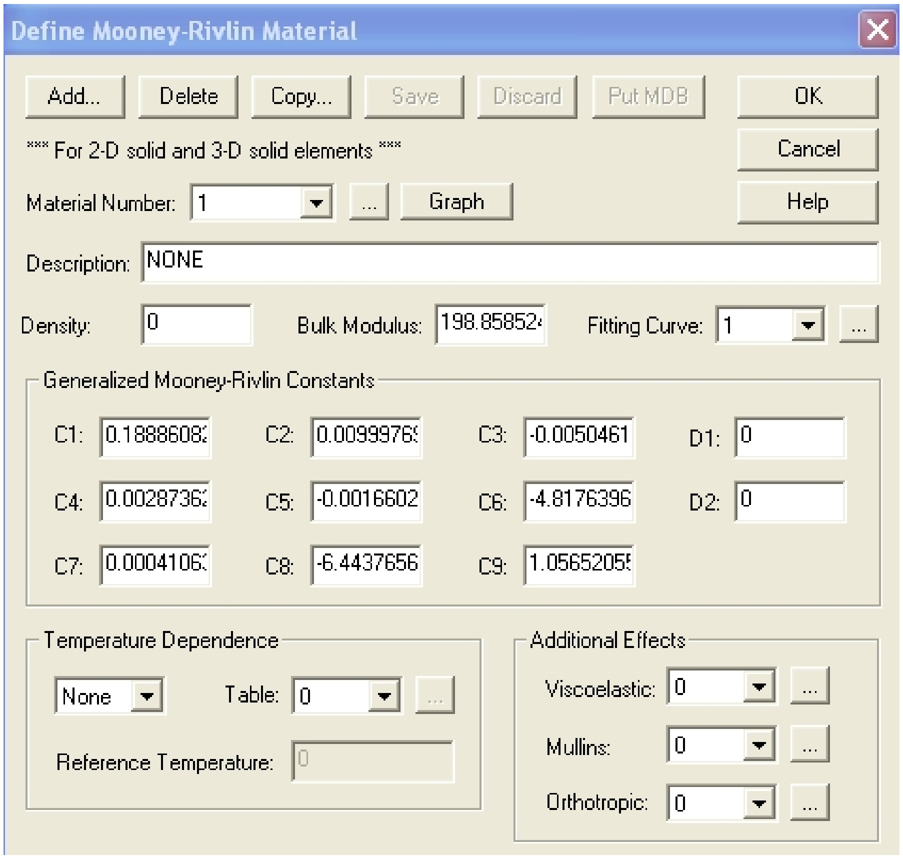

Figure 3.3 Constants of the Mooney-Rivlin model fitted by ADINA

The entire curve fitting for extension-compression experimental data is shown in figure 3.4 while only the curve fitting of the extension part is shown in figure 3.5. Although the extension part of curve-fitting is in good agreement with the experimental data, all the curve fitting settings produce poor curve-fitting results for the compression experimental data. Furthermore, high order approximation does not help at all.

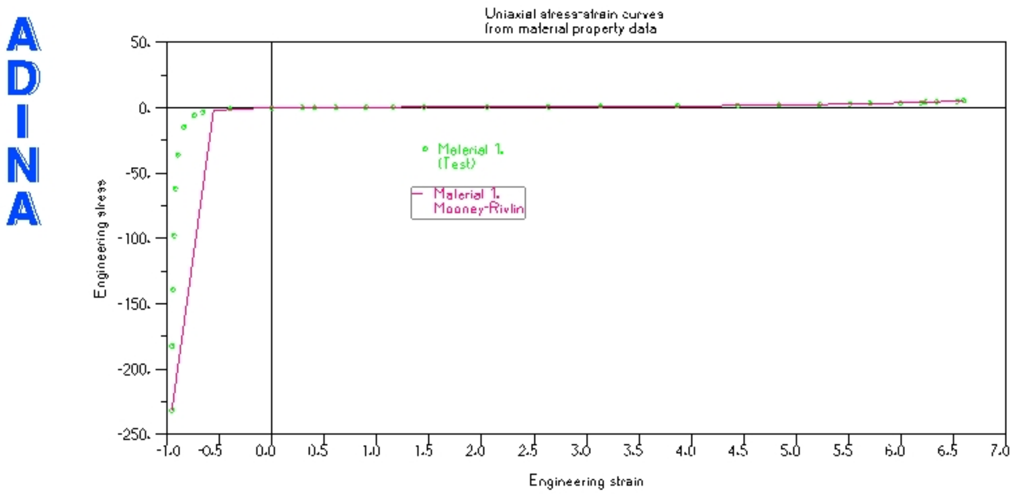

Figure 3.4 Mooney-Rivlin model curve fitting with Gaussian Elimination and order 3 approximation (both extension and compression parts shown)

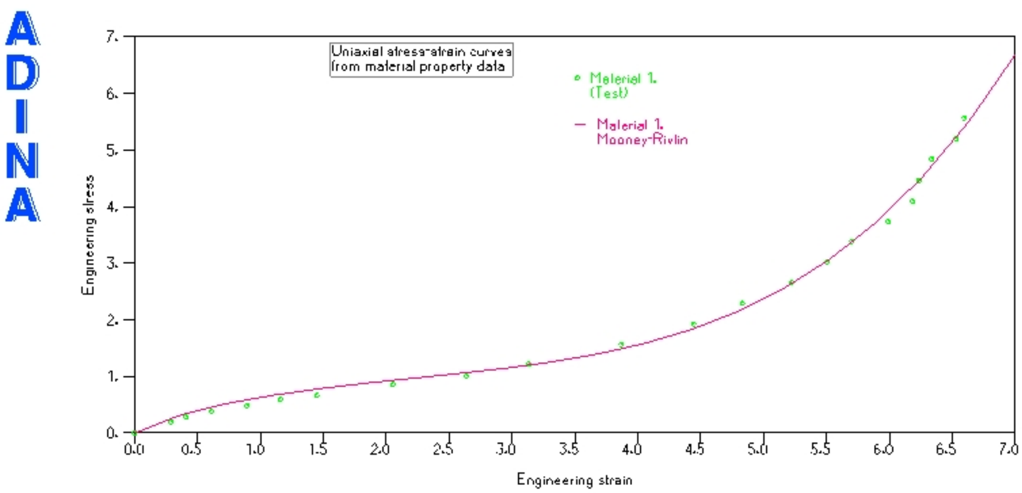

Figure 3.5 Mooney-Rivlin model curve fitting with Gaussian Elimination and order 3 approximation (only extension part shown)

(ii) Arruda-Boyce model

The results from all the different adjustable parameters do not produce any significant difference for Arruda-Boyce model. Hence, SVD is chosen as the “least square solution method” and again the order 3 approximation is employed. The constants of Arruda-Boyce model resulting from curve fitting are shown in figure 3.6.

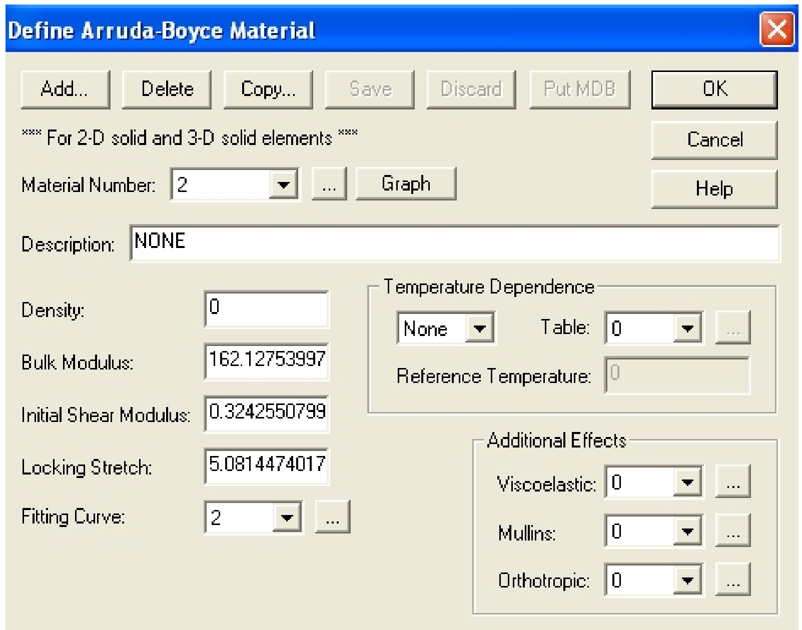

Figure 3.6 Constants of the Arruda-Boyce model fitted by ADINA

The best stress-strain curve fitted from the extension-compression experimental data is shown wholly in figures 3.7 while only the extension part is shown in figure 3.8 respectively. Furthermore, the extension part shows fairly good agreement with the experimental data. As Mooney-Rivlin model, the compression part departs from experimental data largely.

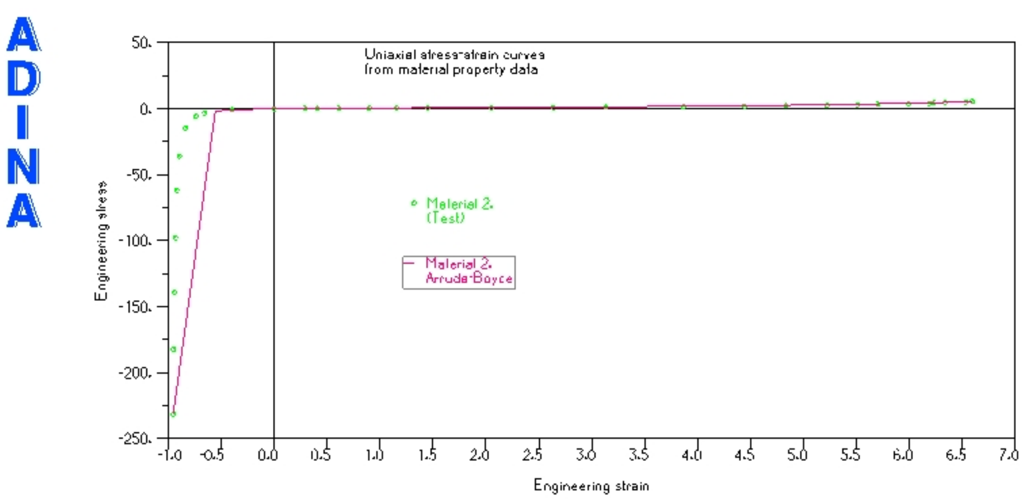

Figure 3.7 Arruda-Boyce model curve fitting with Singular value decomposition and order 3 approximation (both extension and compression parts shown)

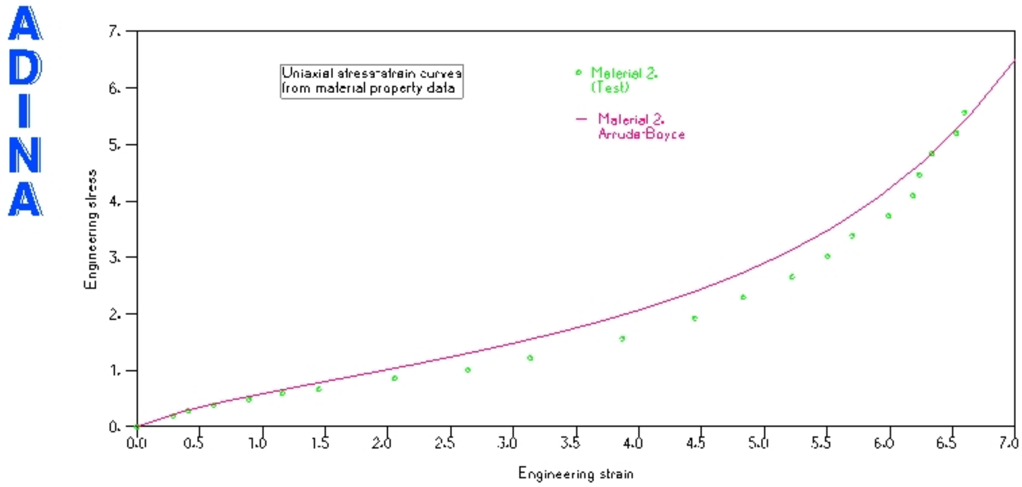

Figure 3.8 Arruda-Boyce model curve fitting with Singular value decomposition and order 3 approximation (only extension part shown)

(iii) Ogden model

The default setting of α is "1 to 9" in ADINA. However, the experimental data can not be fitted well, even for small strain deformation. Hence, as recommended by the ADINA AUI Primer[33], the various α s are set as

$$\begin{cases} \alpha 1 = 0.5; \alpha 2 = -1; \alpha 3 = 1; \ \alpha 4 = -2; \ \alpha 5 = 2; \\ \alpha 6 = -3; \ \alpha 7 = 3; \ \alpha 8 = -4; \ \alpha 9 = 4 \end{cases}$$

and the corresponding best fit curve is obtained using GE and order 9 approximation. The constants are shown in figure 3.9.

The best fitted curve for the extension-compression experimental data is wholly shown in figure 3.10 and the extension part is shown in figure 3.11, which indicates good agreement with experimental data.

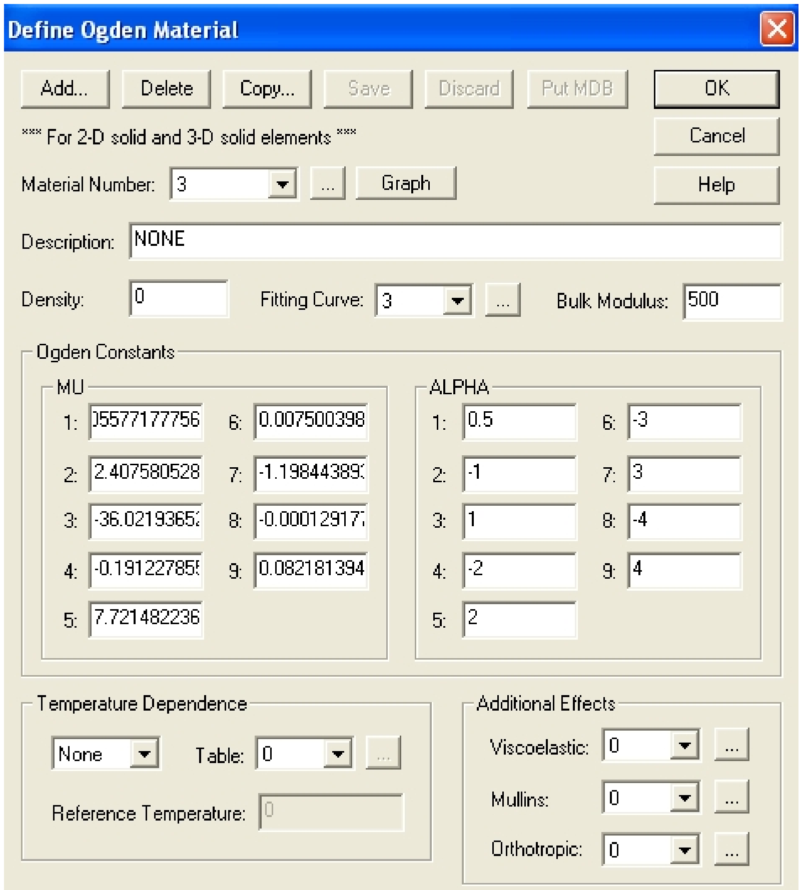

Figure 3.9 Constants of the Ogden model fitted by ADINA

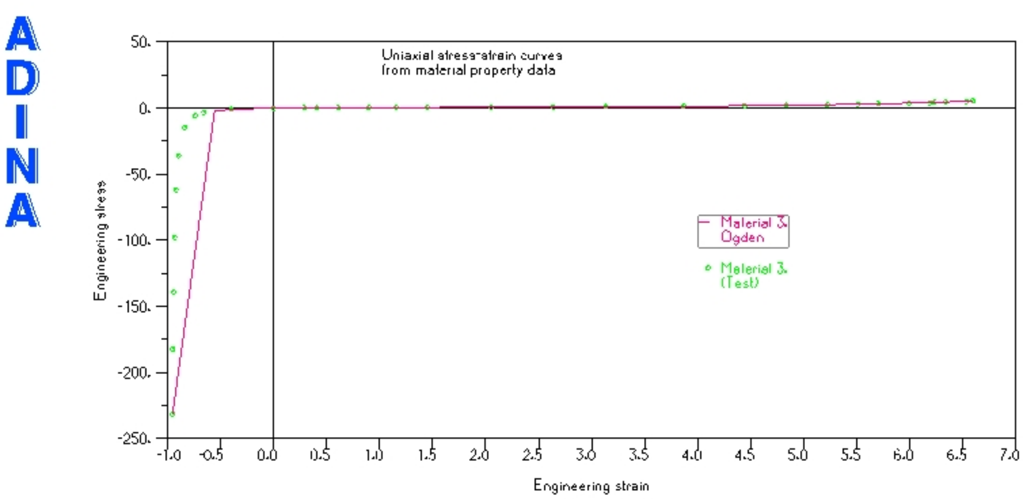

Figure 3.10 Ogden model curve fitting with Gaussian Elimination and order 9 approximation (both extension and compression parts shown)

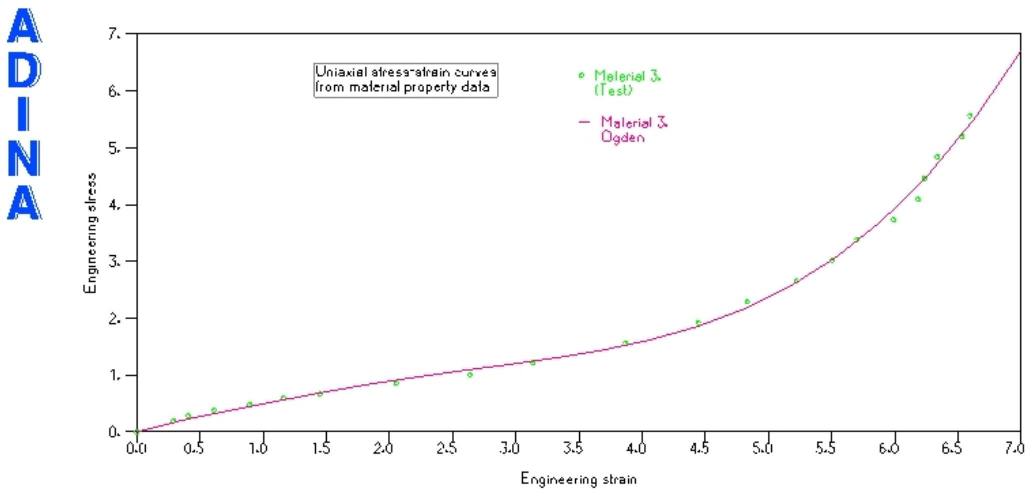

Figure 3.11 Ogden model curve fitting with Gaussian Elimination and order 9.approximation (only extension part shown)

On the other hand, Ogden[34] himself proposed a set of constants which is shown in table 3.2. The resulting uniaxial shear and biaxial deformation stress-strain curves are compared with Treloar's data in figure 3.12 and figure 3.13 respectively, and both curves are relatively close to experimental data.

Table 3.2 Ogden's constants

	α	μ
1	1.3	0.6173486
2	5	0.0012422
3	.2	.0.009813

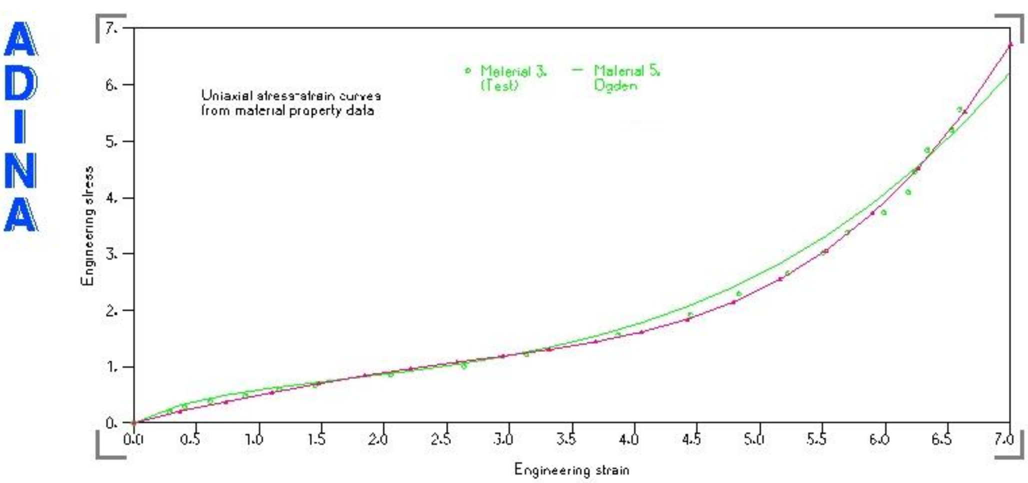

Figure 3.12 Ogden model uniaxial stress-strain relation (green curve) compared with experimental data (green dot/red curve)

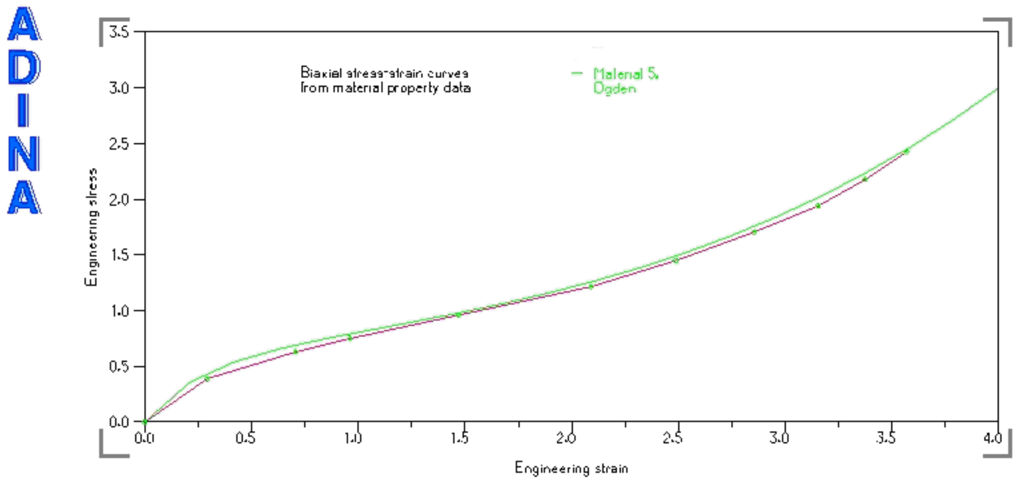

Figure 3.13 Ogden model biaxial stress-strain relation (green curve) compared with experimental data (green dot/red curve)

(iv) Sussman-Bathe model

There is no parameter to fit in Sussman-Bathe model. However, this model gives a perfect fit to the experimental data, ranging from compression to extension. Furthermore, it gives a good fit for small strain deformation.

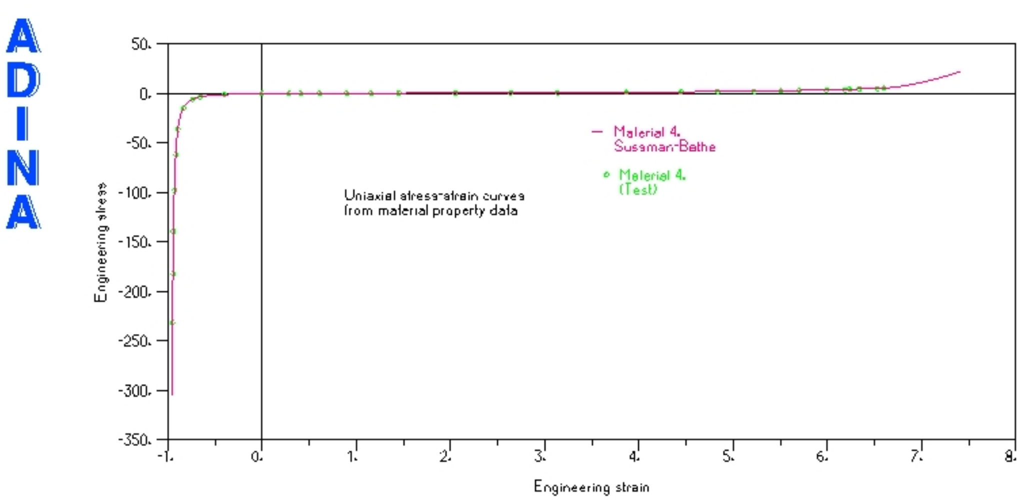

Figure 3.14 Sussman-Bathe model curve fitting (full strain range)

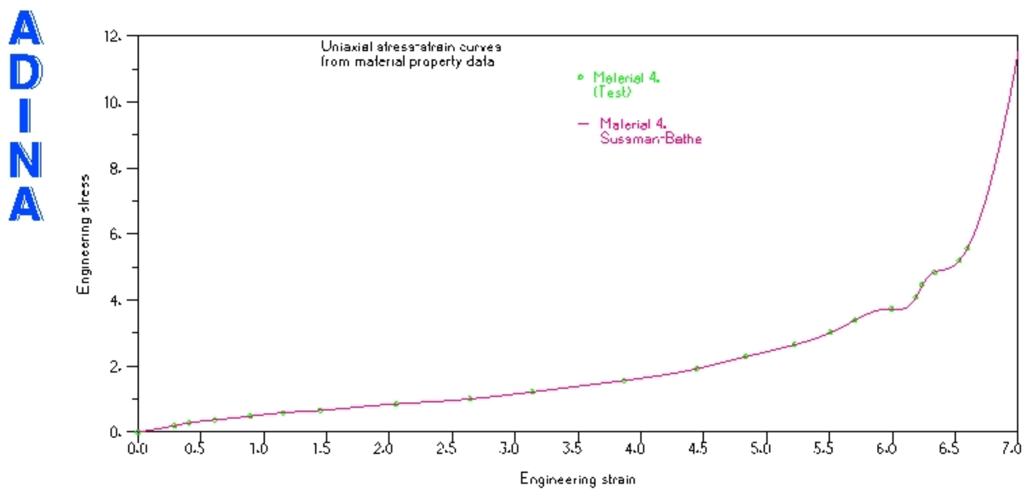

Figure 3.15 Sussman-Bathe model curve fitting (strain from 0 to 5)

From above fitting results, it is clearly shown that only the Sussman-Bathe model produces an accurate curve fit. This is evident in the compression experimental data where all other models, except the Sussman-Bathe model, fail to produce appropriate approximations.

3.1.2 Verification of predicted pure shear deformation curve

In order to verify the correctness of the rubber material models, except the capability to fit the uniaxial compression and extension experimental data, the predictability of pure shear deformation and other general deformations must be considered as well. Only if all the deformations can be predicted accurately, the model can be considered as correctly proposed.

Here first the predictive capability of pure shear deformation is studied. The pure shear experimental data from Treloar are used as shown in Table 3.3. In all cases, the constants for the models determined in the previous section 3.1.1 are used.

Table 3.3 Pure shear experimental data from Treloar

Engineering strain	Engineering stress
0	0
0.4874	0.4133
0.8697	0.591
1.3498	0.7734
1.9848	0.9219
2.522	1.0898
3.0021	1.2529
3.4332	1.4545
3.7505	1.6034
4.0187	1.786

(a) Mooney-Rivlin model

The shear curve using the Mooney-Rivlin model is plotted in figure 3.16 and it is close to the experimental data when the strain is small and obviously quite different from experimental data when the strain becomes larger.

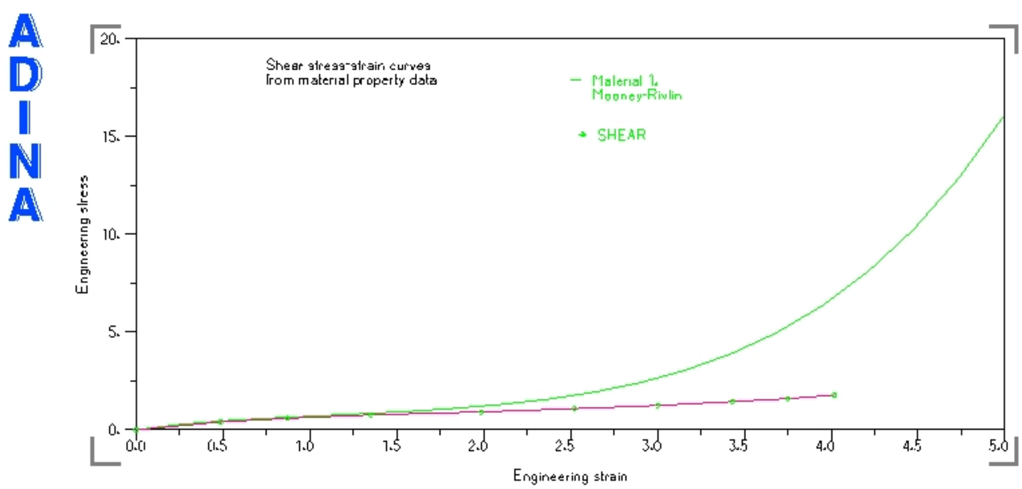

Figure 3.16 Mooney-Rivlin model shear stress-strain relation curve (green curve) vs experimental data (green dot/red curve)

(b) Arruda-Boyce model

As shown in Figure 3.17, compared to the Mooney-Rivlin model, the Arruda-Boyce model is able to predict the shear curve better, although it is still steeper than the experimental data.

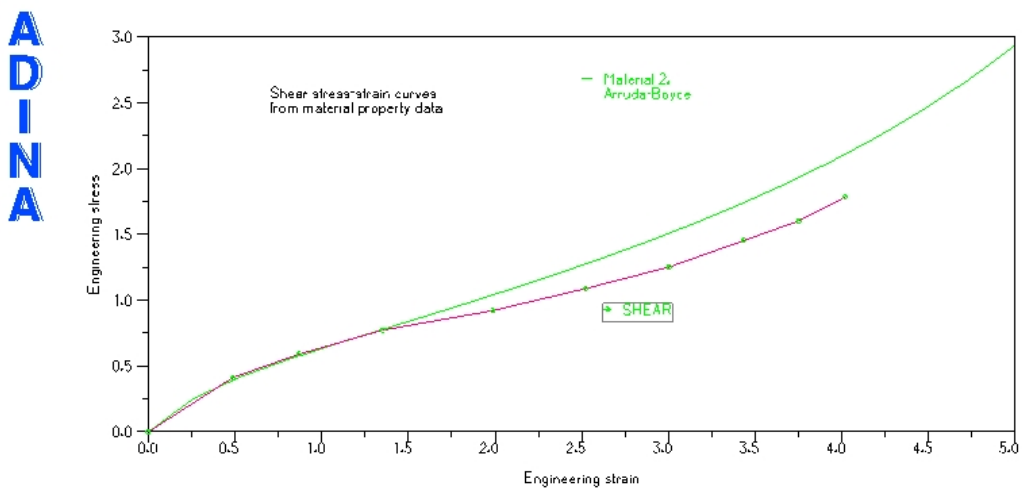

Figure 3.17 Arruda-Boyce model shear stress-strain relation curve (green curve) vs data (green dot/red curve)

(c) Ogden model

The shear curve from the Ogden model using both ADINA's and Ogden's constants are compared with the experimental data, as shown in figure 3.18.

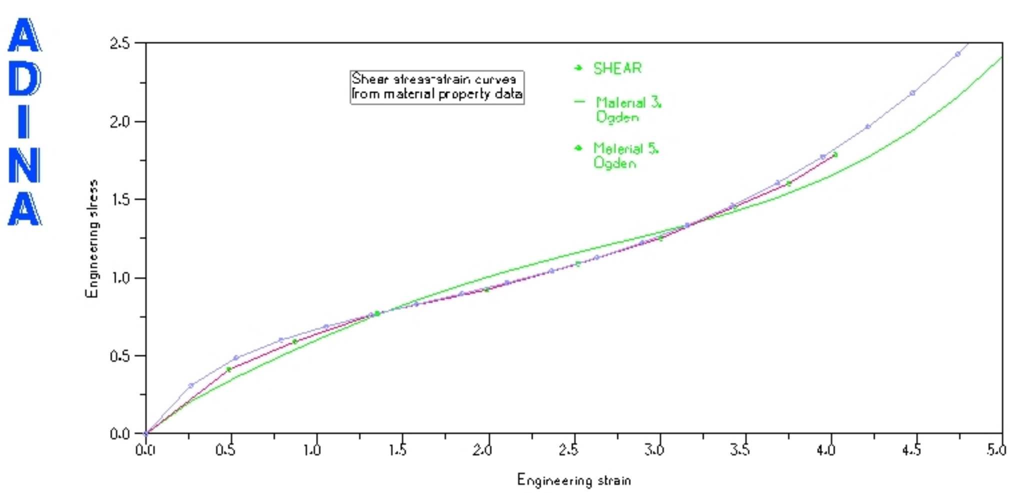

Figure 3.18 Ogden model shear stress-strain relation curve (green curve: ADINA's constants; purple curve: Ogden's constants) compared with experimental data (green dot/red curve)

From the comparison in figure 3.18, the Ogden model using Ogden's constants offers a better fit for shear deformations. As shown in figure 3.12, 3.13 and 3.18, using the same experimental data, different stress-strain curves could be produced by selecting different approximation order, least square solution method and values of α s. Hence, different individual preferences of curve fitting parameters will result in different model constants and thus different simulation results for the same problem. A good fitting result is therefore difficult to obtain. On the other hand, with the Sussman-Bathe model, a very good result can be obtained easily.

(d) Sussman-Bathe model

The most accurate result is achieved from the Sussman-Bathe model, whose shear curve is very close to the experimental data, even when the strain is large.

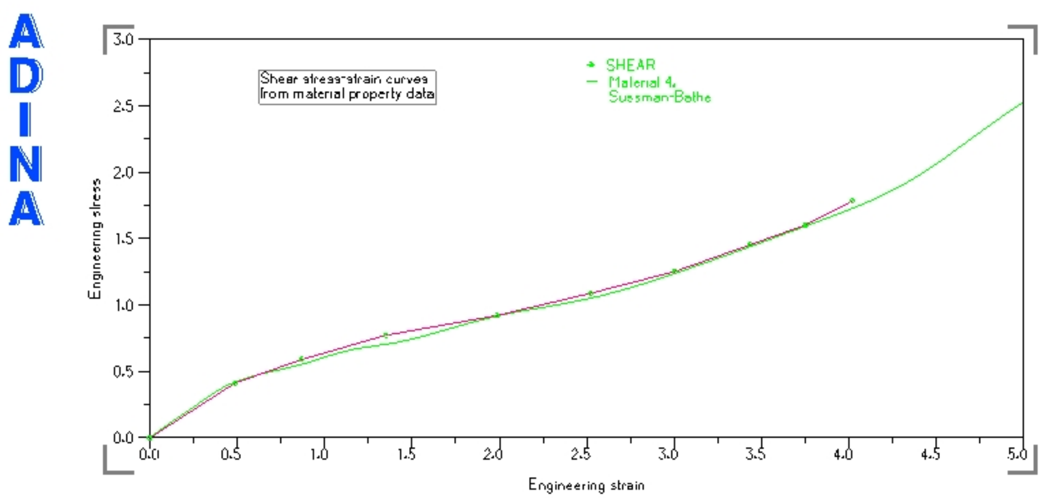

Figure 3.19 Sussman-Bathe model shear stress-strain relation curve (green curve) vs experimental data (green dot/red curve)

3.2 Non-homogenous deformation investigation

3.2.1 Experiment and numerical model settings

The experimental specimens and finite element model are built as shown in figure 3.20.

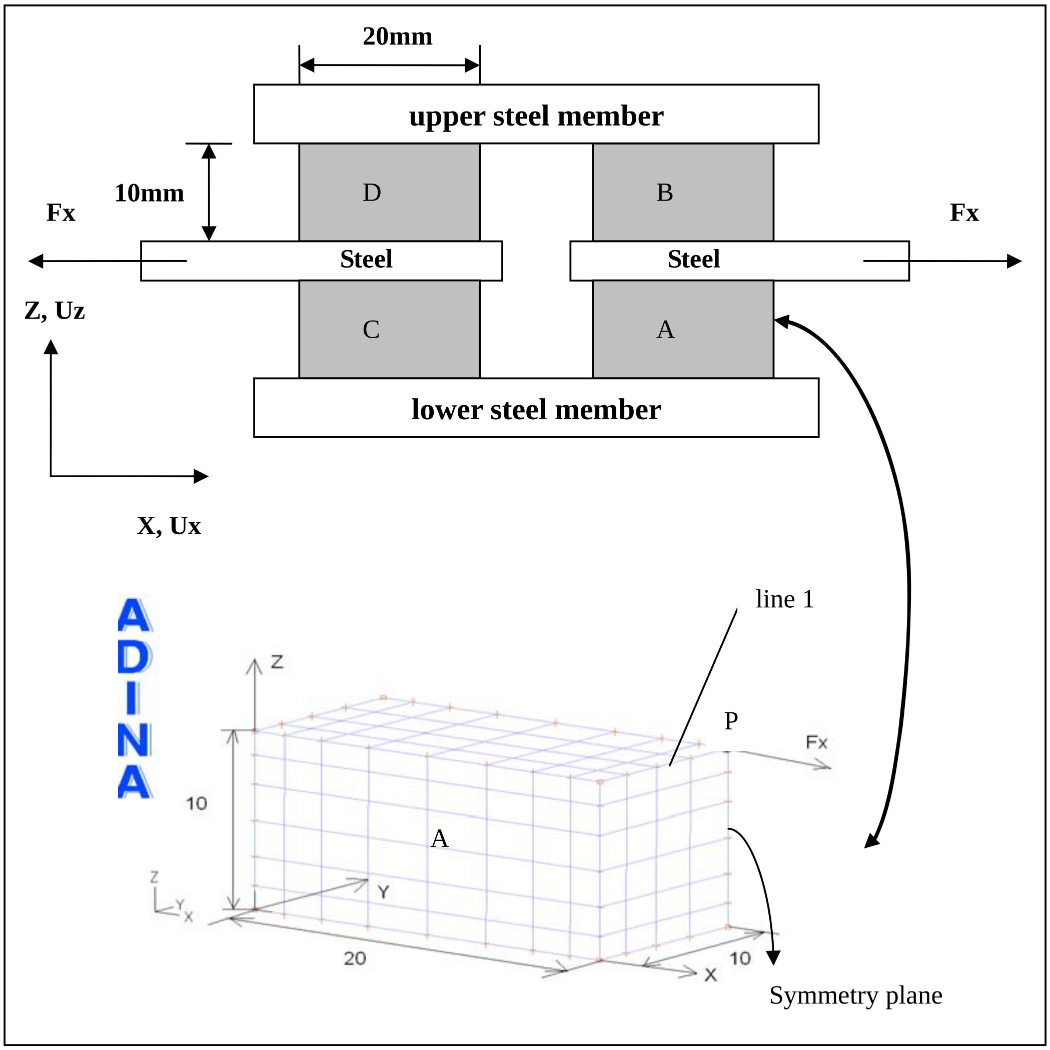

Figure 3.20 experimental setting of P.A.J. van den Bogert and R. de. Borst [10] (upper part) and FEM model in ADINA (lower part)

(a) Descriptions of non-homogenous shear deformation experiment

A composition of four identical specimens (A, B, C and D) through a rigid connection with steel members at the upper and lower faces is built as shown in upper part of figure 3.20. In the middle of the steel members, a horizontal displacement has been imposed. In addition, these specimens are free to deform in Z-direction. Each of the four experimental specimens (A, B, C, D) has a dimension of 20mm by 20mm by 20mm.

(b) FEM model Geometry and boundary condition descriptions

Exploiting the symmetry of the experimental settings, only half of the lower right block (A) is meshed as the computational domain in the FEM model whose dimension now is 20mm by 10mm by 10mm.

Corresponding to the experimental setting, the boundary and loading conditions for the computational domain are as follow: the bottom plane is subjected to Dirichlet boundary condition in all three directions; the y-displacements of both the top and symmetry plane (y=10mm) are similarly subjected to Dirichlet boundary condition due to symmetry; the top plane is allowed to move rigidly in both the x and z-directions as they are constrained by the upper right corner node P where the shear force F_x is applied. The point force F_x on point P, together with the displacement constraint of top plane to the loading point P, is equivalent to a line force on line 1 as shown in figure 3.20.

(c) Material model settings

The Mooney-Rivlin, Arruda-Boyce, Ogden and Sussman-Bathe models are employed to carry out the numerical analysis. As discussed in previous chapter, the uniaxial test data are needed to build these models in ADINA. The data of a uniaxial elongation experiment, first carried out by P.A.J. van den Bogert and R. de. Borst[10], is shown in figure 3.21.

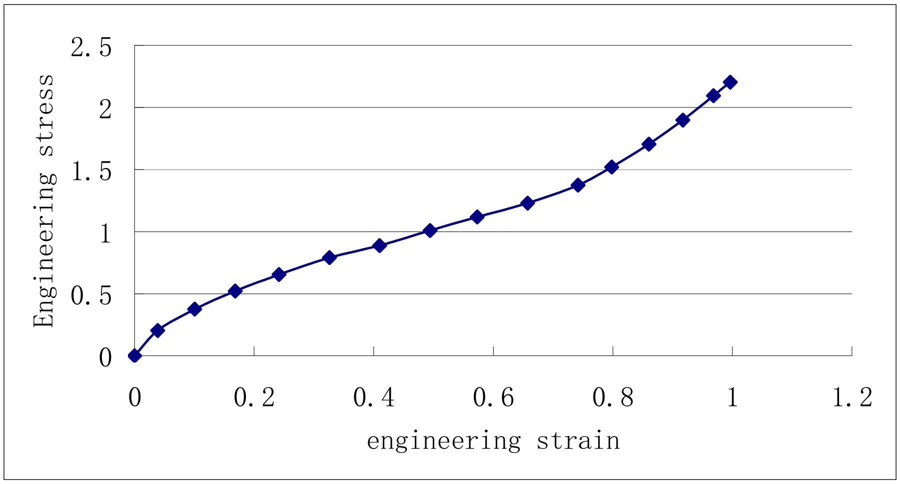

Figure 3.21 Uniaxial experimental results of P.A.J. van den Bogert and R. de. Borst

Because of the theoretical limitation of the Mooney-Rivlin model, P.A.J. van den Bogert and R. de. Borst limited its valid scope to $0.15 \le \varepsilon \le 0.5$ when the constants are fitted for the Mooney-Rivlin model. For the Ogden model, a larger range of $0 \le \varepsilon \le 1$ was used. Since the experimental error is relatively large in the neighborhood of $\varepsilon = 0$, it is reasonable to use the data ranging from $0.15 \le \varepsilon \le 1$. The model constants, reproduced from P.A.J. van den Bogert and R. de. Borst's paper[10] and P.A.J. van den Bogert's PhD thesis[35], are given in table 3.4.

Table 3.4 Constants of various models

	Mooney-Rivlin model	C1	C2			Bulk modulus
a-fit	5^{th} cycle $0.15 \le \varepsilon \le 0.5$	0.1486	0.4849			1.267
	Ogden model	$\mu 1$	$\alpha 1$	$\mu 2$	$\alpha 2$	Bulk modulus
a-fit	$0.15 \le \varepsilon \le 1$	.1.443	.1.787	2.741e.3	9.581	1.303
b-fit	$0.15 \le \varepsilon \le 1$	.0.9952	.2.713	2.053e.3	9.905	1.360
c-fit	Pos. powers $0.15 \le \varepsilon \le 1$	3.164	0.5	0.0486	5.5	0.925
e-fit	$0.15 \le \varepsilon \le 1$	.2.784	.0.8632	3.114e.3	9.411	1.2205

For Mooney-Rivlin model, a much better uniaxial curve fitting could be achieved with ADINA by employing the Gaussian Elimination least square solution, as shown in figure 3.22. It clearly fits the experimental data much better than P.A.J. van den Bogert and R. de. Borst's (green line in figure 3.22). However this curve performs poorly if the range is extended to $0 \le \varepsilon \le 3$, as shown in figure 3.23. The stress value actually decreases and becomes negative when strain is increased from 1 to 2, which is not physically possible.

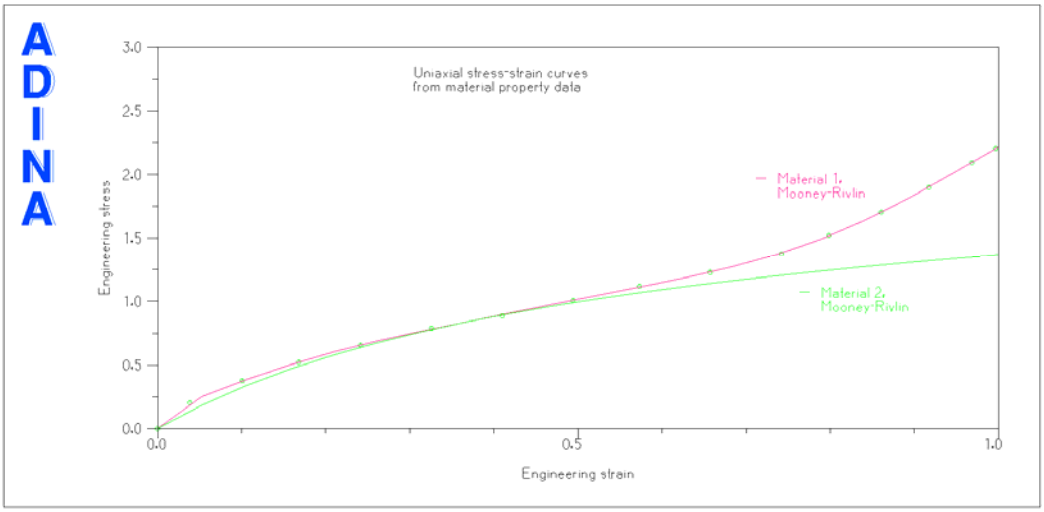

Figure 3.22 Mooney-Rivlin model uniaxial curve fitting compared with experimental data

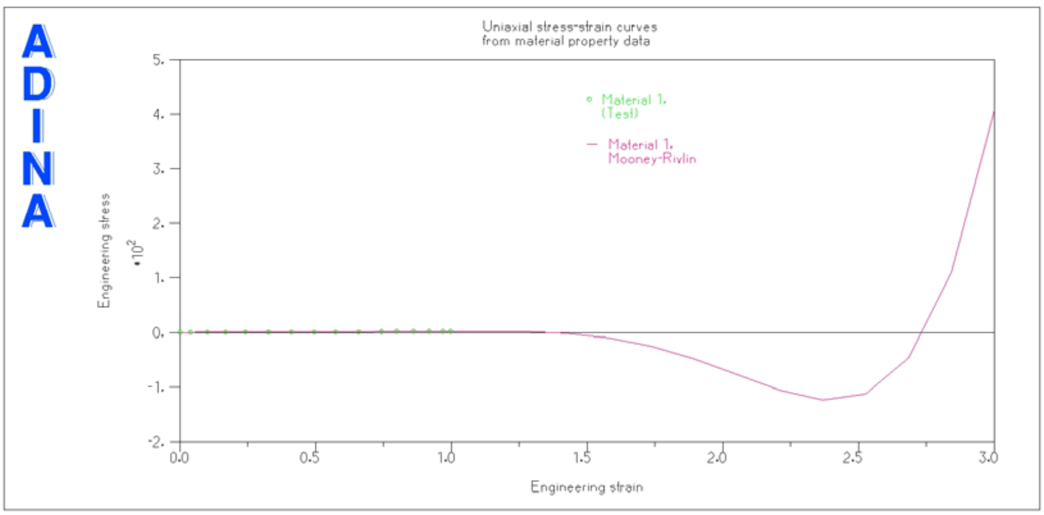

Figure 3.23 Mooney-Rivlin model with constants fitted by Gaussian Elimination shown in a larger scope

If the Singular Value Decomposition least square method is employed instead, a worse stress-strain curve, as shown in figure 3.24 is achieved. Thus for the Mooney-Rivlin model, P.A.J. van den Bogert and R. de. Borst's constants produce a better fitting compared to constants fitted directly from ADINA with either Gaussian Elimination or Singular Value Decomposition, and are directly employed in the following analysis.

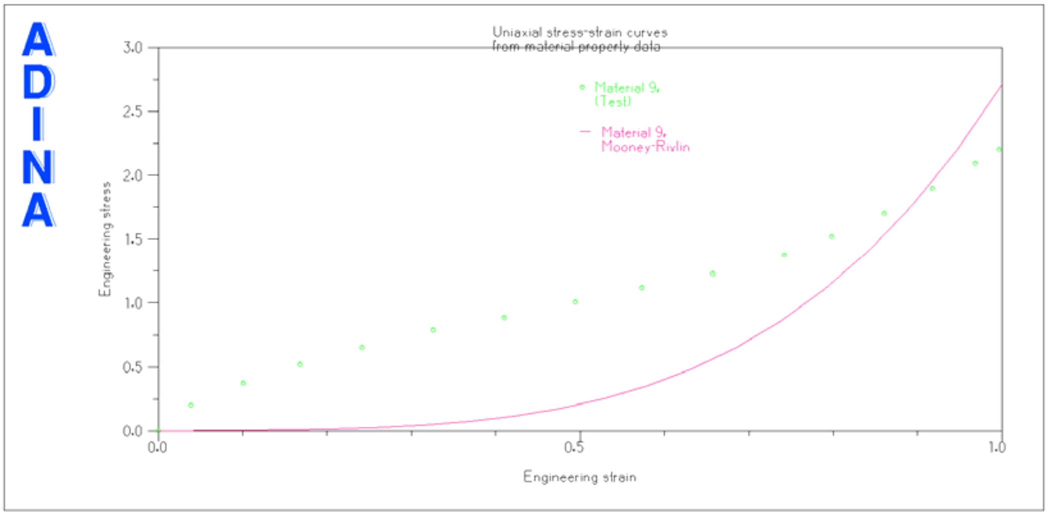

Figure 3.24 Stress-strain relation for Mooney-Rivlin model with constants fitted by Singular value decomposition

With P.A.J. van den Bogert and R. de. Borst's uniaxial experimental data, an Ogden material model (material no. 4 in figure 3.25) is built directly with ADINA. Its uniaxial curve fitting is compared with other models given in P.A.J. van den Bogert and R. de. Borst's paper: Mooney-Rivlin model with "a-fit" is built as material no. 2; Ogden model with "a-fit" as material no. 5, "b-fit" as material no. 6, "c-fit" as material no. 7, and "e-fit" as material no. 8.

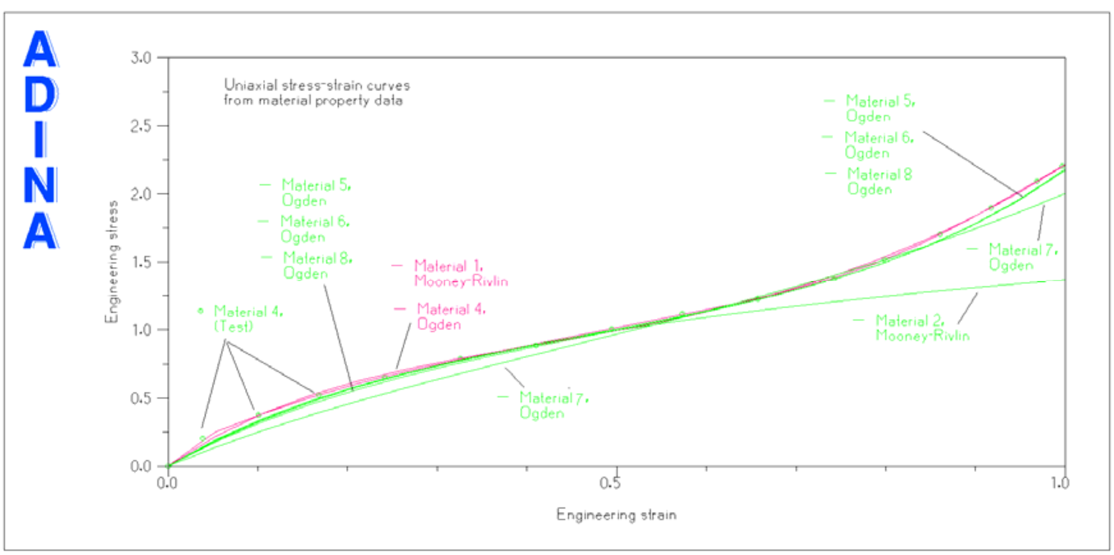

Figure 3.25 Fitting of stress-strain data with different models

From figure 3.25, Ogden model directly fitted by ADINA (no. 4) gives the best fitting of the experimental data with a strain from 0 to 1. a-fit, b-ftt and e-fit Ogden models (no. 5,6,8 curves) give acceptable fitting, Ogden model (no. 7 curve) with all-positive αs gives a larger departure while Mooney-Rivlin model (no. 2 curve) produces the largest error. However, regarding the uniaxial compression part as shown in figure 3.26, large differences between various curves are observed even for Ogden material model no. 5, no. 6 and no. 8 which are quite close for extension part.

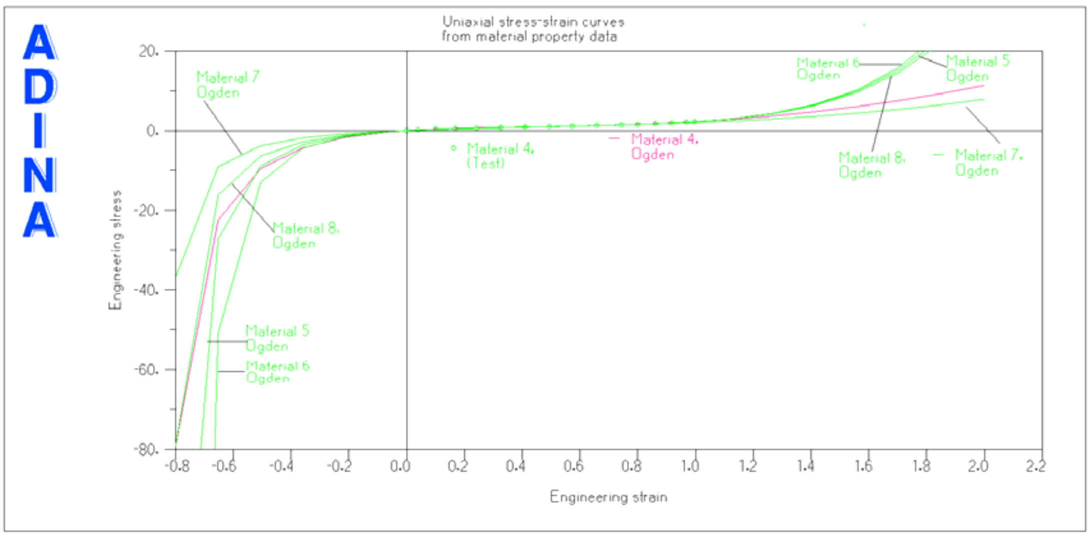

Figure 3.26 Fitting of stress-strain data with different models in a larger scope

Furthermore, the predicted pure shear stress-strain relation, as shown in figure 3.27, is quite different when the strain increases above 1 or when the material is under compression.

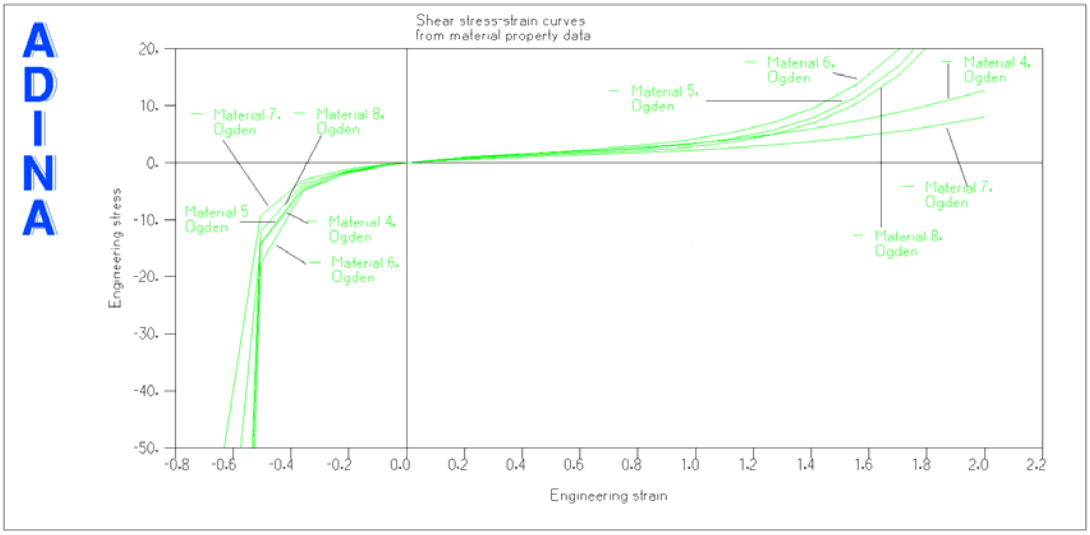

Figure 3.27 Ogden model shear stress-strain curve

P.A.J. van den Bogert and R. de. Borst's experiment is quite limited; especially there is no experimental data for compression. Building a Sussman-Bathe model is meaningless if there is no compression data. From previous discussion, generally, Ogden modes give better curve-fitting for experimental data. It is evident that, except Ogden model with c-fit (no. 7 curve), all Ogden models fit experimental data well within the valid range of $0.15 \leq \varepsilon \leq 1$. However, although the c-fit Ogden model with all positive powers produces the worst fitting, it is the only Ogden model which is stable for all three deformations (referring to chapter 4). Hence, the c-fit Ogden model is still used to build another Sussman-Bathe model for comparison. Therefore, data from the uniaxial curve of a-fit Ogden model (no. 5 curve), c-fit Ogden model (no. 7 curve) and Ogden model (no. 4 curve) are used to build the Sussman-Bathe model as no. 11, 12 and 10 models respectively. Their uniaxial and shear deformation stress-strain curves are plotted in figure 3.28 and 3.29.

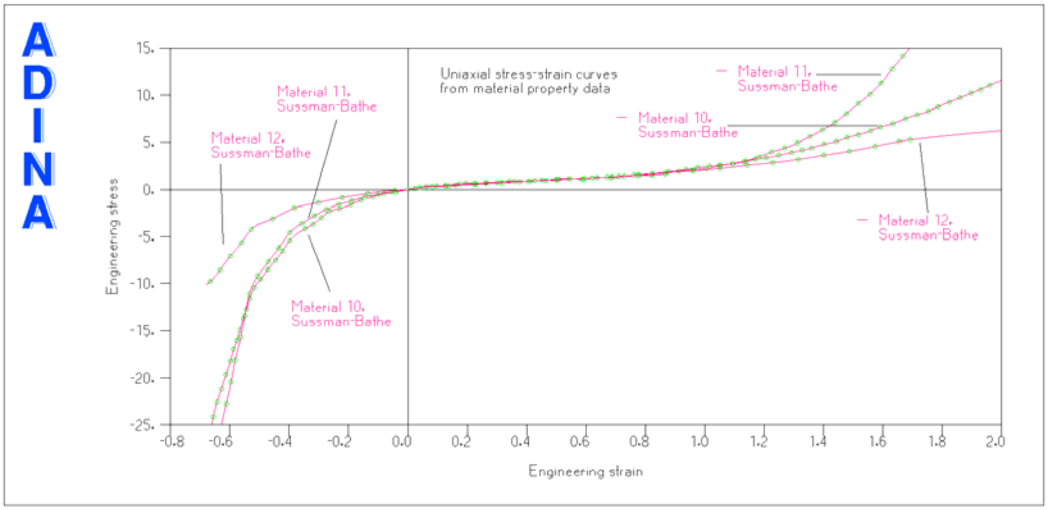

Figure 3.28 Uniaxial deformation stress-strain curves of the Sussman-Bathe models

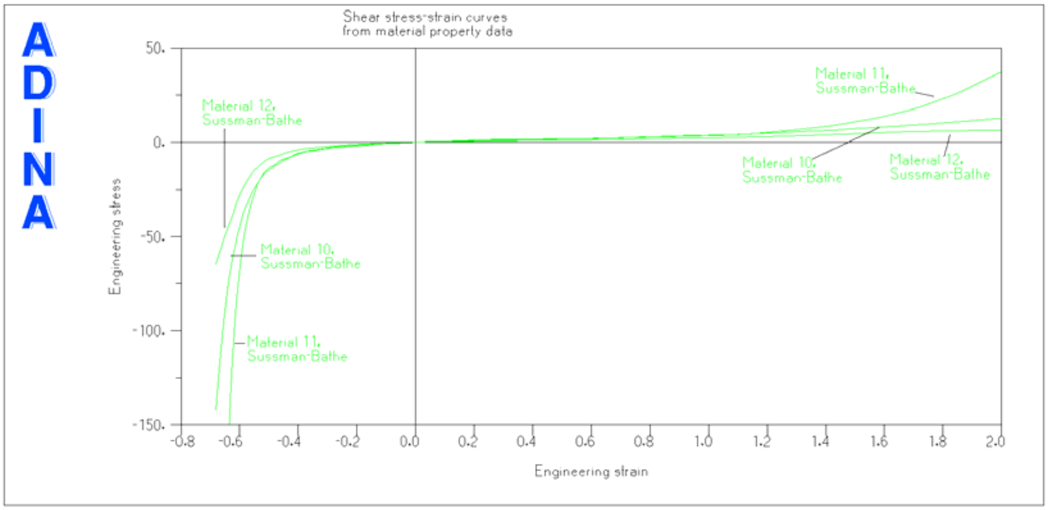

Figure 3.29 Shear deformation stress-strain curves of the Sussman-Bathe models

Comparing the curves of Sussman-Bathe models with their corresponding Ogden models, it's obvious that they are quite similar.

Furthermore, with the uniaxial elongation experimental data, an Arruda-Boyce model is built and it fits the experimental data well, as shown in figure 3.30.

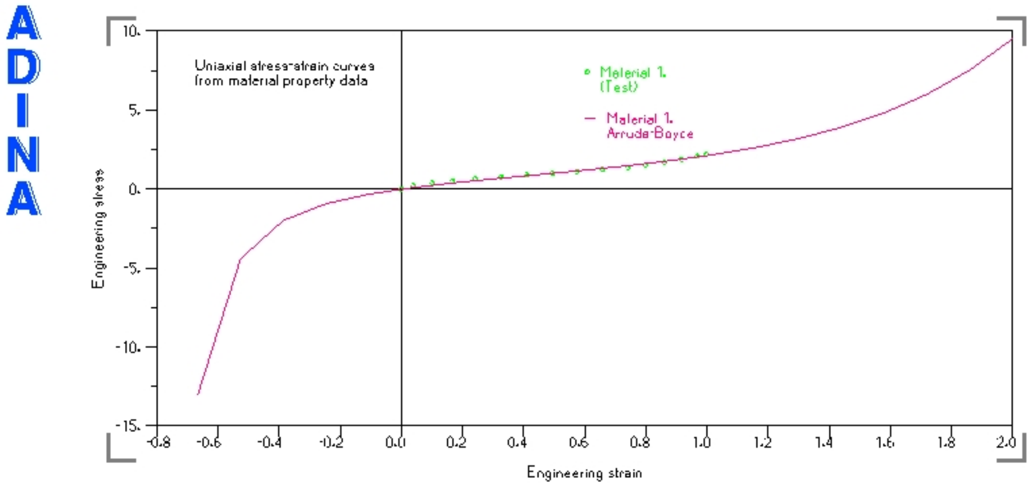

Figure 3.30 Stress-strain relation of the Arruda-Boyce model

3.2.2 Non-homogenous shear deformation simulation results

A stress distribution plot in figure 3.31 shows the general deformation results of the non-homogenous shear deformation.

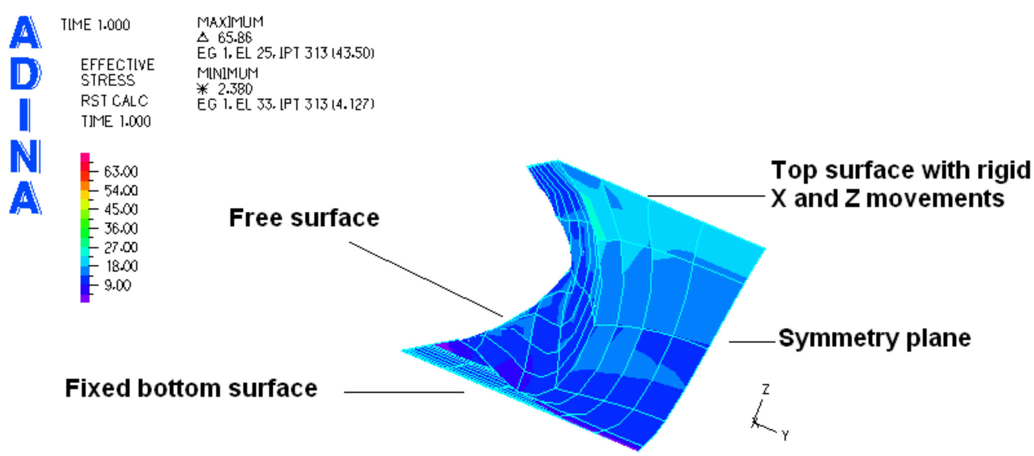

Figure 3.31 Non-homogonous shear deformation simulation results

(a) Mooney-Rivlin model

The x-displacement and z-displacement of the Mooney-Rivlin model with respect to applied force F_x are shown in figure 3.32.

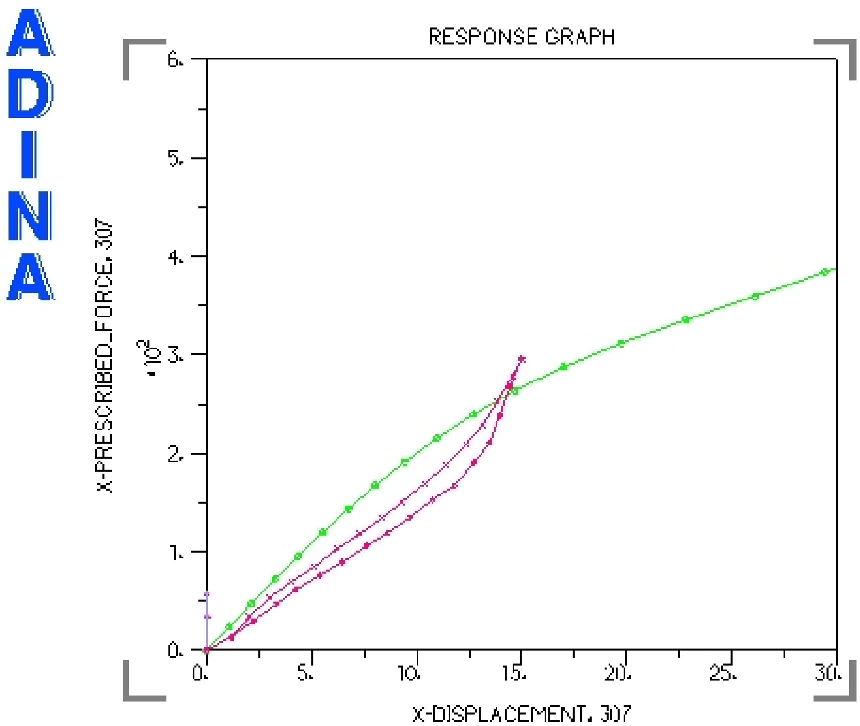

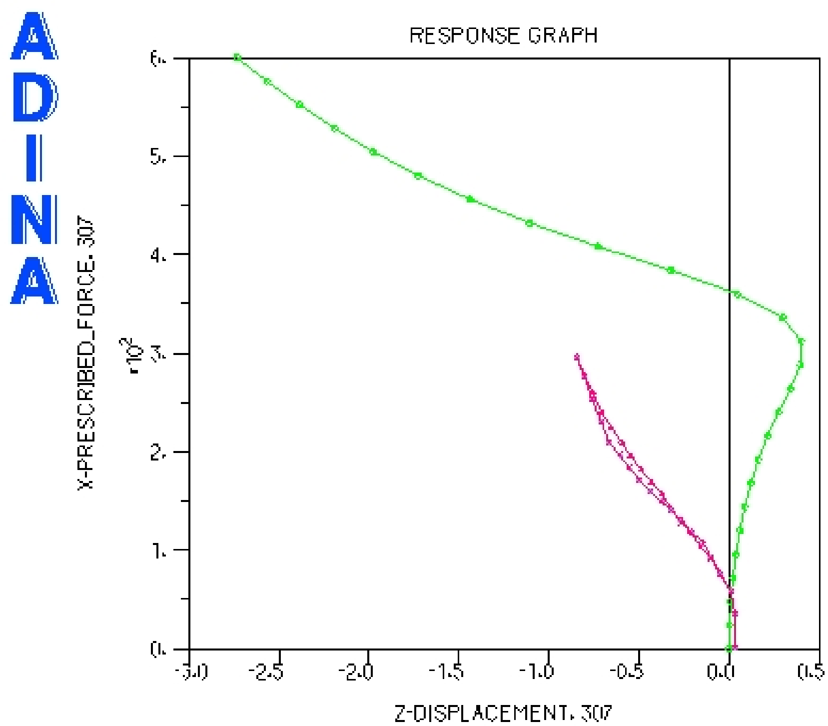

Figure 3.32 X-displacement (top) and z-displacement (bottom) with respect to applied force; Mooney-Rivlin model: green curve, experimental data: red curve

For x-displacement, although the Mooney-Rivlin model produces a correct deformation trend, there is a large difference between the simulation and experimental results, especially when the strain becomes larger.

For z-displacement, experimental results indicate that it should always be negative. However, Mooney-Rivlin model produces positive z-displacement at the beginning and then the positive strain increases till 0.4, which is obviously not a physically correct result. Although z-displacement of the Mooney-Rivlin model turns into negative at last, its value is much higher than the experimental data.

(b) Ogden model

The x-displacement and z-displacement of the Ogden models with respect to the applied force are shown in figure 3.33.

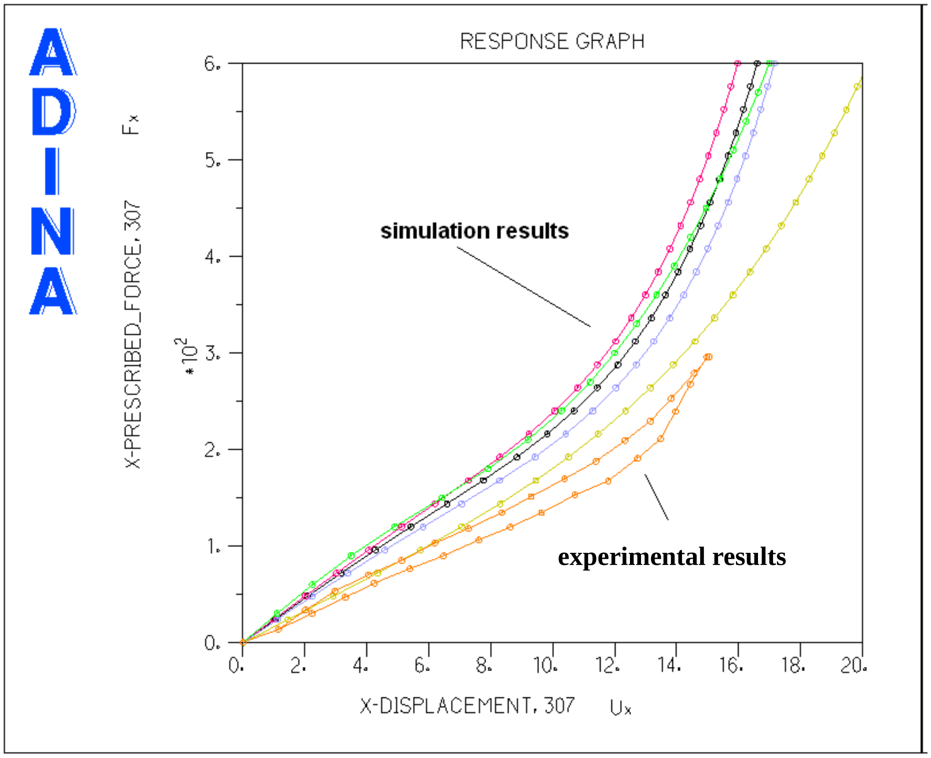

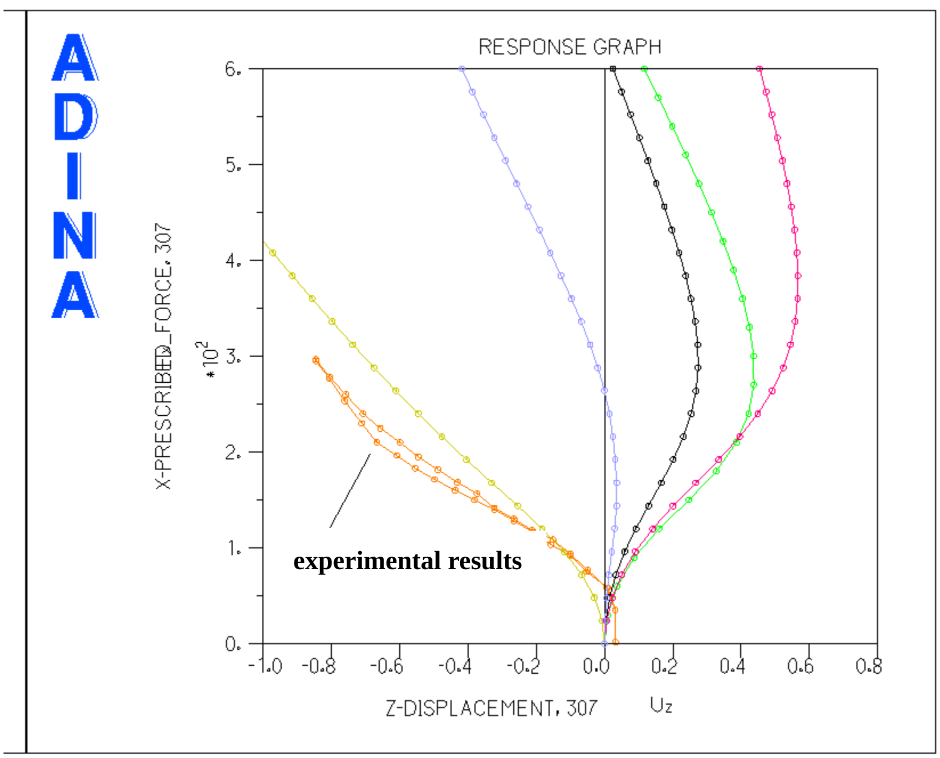

Figure 3.33 X-displacement (top) and z-displacement (bottom) with respect to the applied force. Ogden a-fit model: black curve; Ogden b-fit model: red curve Ogden c-fit model: yellow curve; Ogden e-fit model: blue curve Ogden model fitted by ADINA: green curve; experimental data: orange curve

It is observed that all the Ogden models predict the x-displacement trend correctly. Among five Ogden models, the model with all positive powers (c-fit) produces a simulation result which is closest to the experimental data for the x-displacement. Furthermore, it is also the model with all positive powers (c-fit) that represents a physically correct z-displacement which should always be negative. The e-fit Ogden model generates similar results as Mooney-Rivlin model for z-displacement. It is positive at the beginning and ends up with a negative value which is much higher than experimental data. Other three Ogden models produce completely wrong z-displacement which is always positive within the whole loading range.

(c) Sussman-Bathe model

The x-displacement and z-displacement of the Sussman-Bathe models with respect to the applied force are shown in figure 3.34.

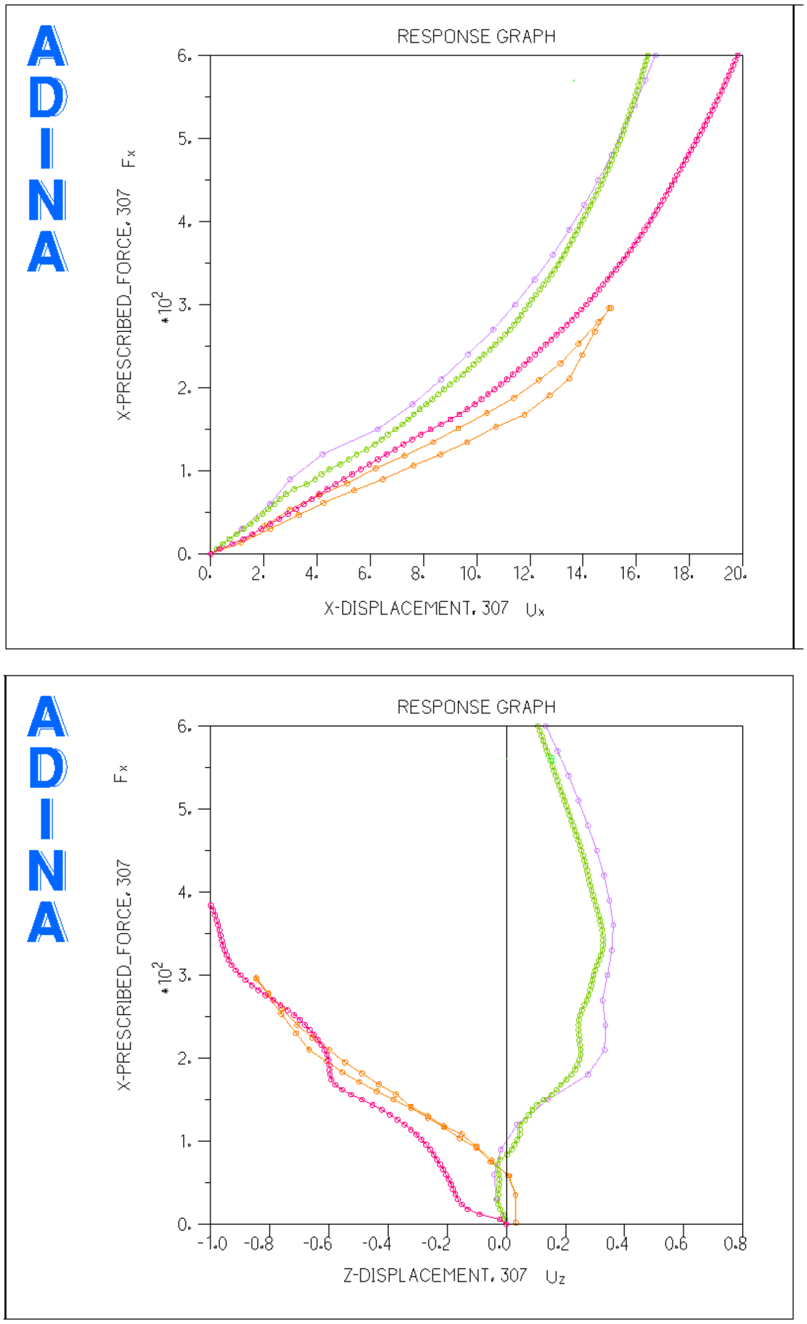

Figure 3.34 X-displacement (top) and z-displacement (bottom) with respect to applied force of Sussman-Bathe model with a-fit data: Green curve; c-fit data: red curve; data fitted from Ogden model 4: blue curve; Experimental data: orange curve

The Sussman-Bathe model which was built through the Ogden c-fit data gives the closest simulation result for x-displacement. In addition, it is also the only model which produces physically correct z-displacements. Especially as the external force increases, the predicted z-displacement gets closer to the experimental data. On the other hand, the z-displacements of the other two Sussman-Bathe models, which are built from a-fit Ogden model and no. 4 Ogden model, are still physically not reasonable.

There are large differences for the compression stress-strain curve for the three Ogden models which Sussman-Bathe models are built from. Although their extension curve is similar, the differences in compression curve introduce great divergence between three Sussman-Bathe models. It also proves the idea of Sussman and Bathe that both extension and compression data are required to build a correct model[8].

(d) Arruda-Boyce model

The x and z-displacement with respect to the applied force for the Arruda-Boyce model and experimental data are shown in figure 3.35.

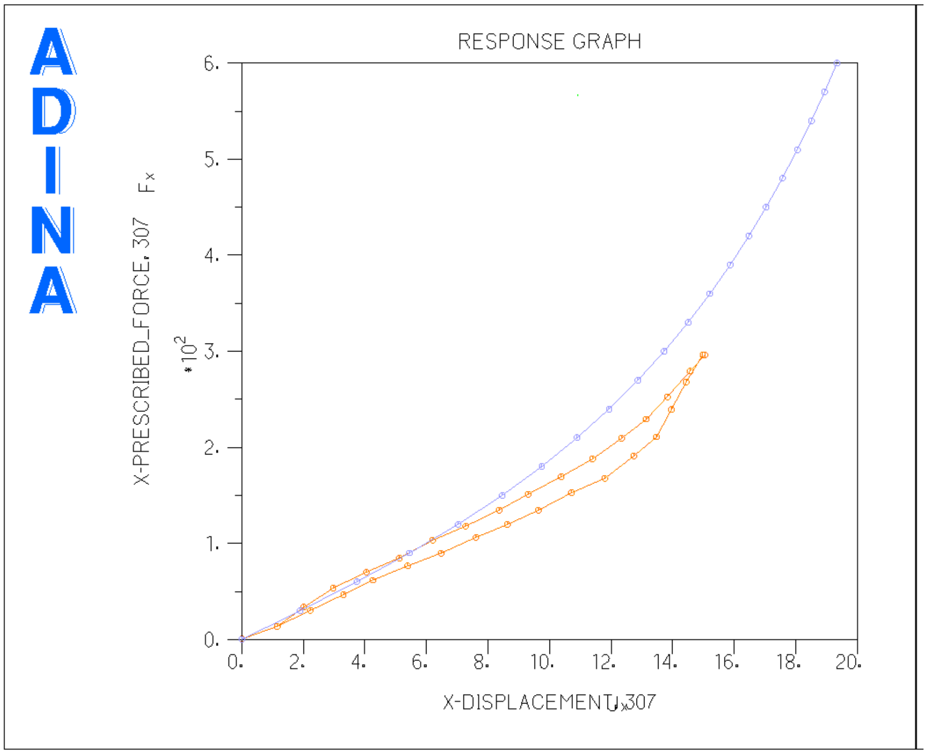

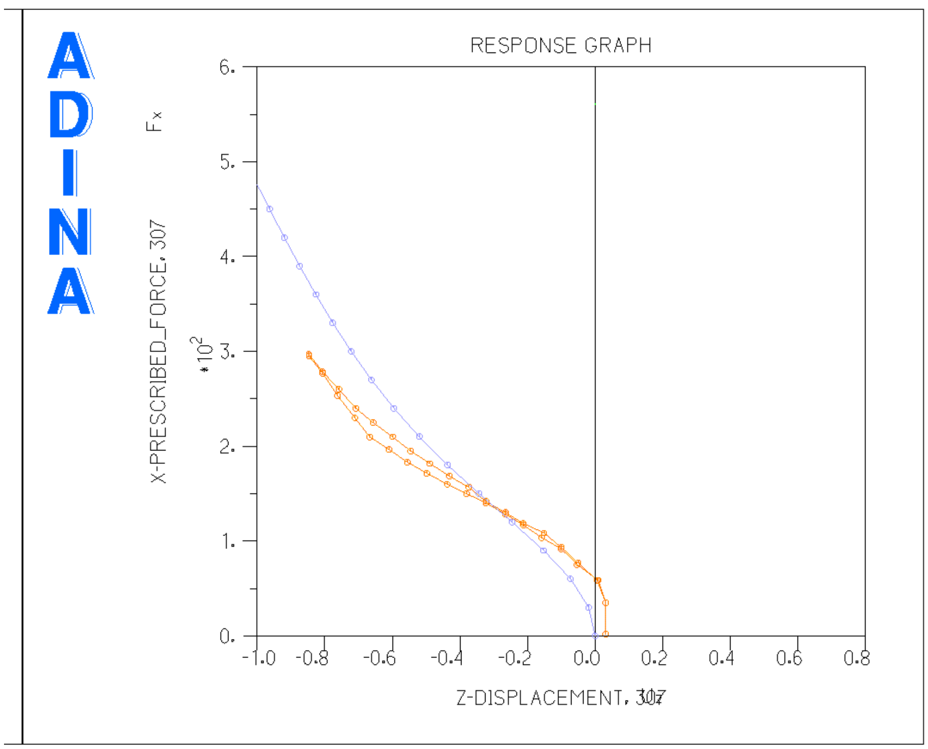

Figure 3.35 X-displacement (top) and z-displacement (bottom) with respect to applied force of Arruda-Boyce model with blue curve for simulation results and orange curve for experimental data

It is observed that Arruda-Boyce model produces correct results for both x-displacement and z-displacement. Furthermore, their values are also quite close to experimental data.

From the above comparison, while all models produce x-displacement with correct trend but only the c-fit Ogden model, Arruda-Boyce model and Sussman-Bathe (built from c-fit Ogden model) produce reasonable z-displacement. The x-displacement and z-displacement simulation results of above three models are shown in figure 3.36, together with experimental data.

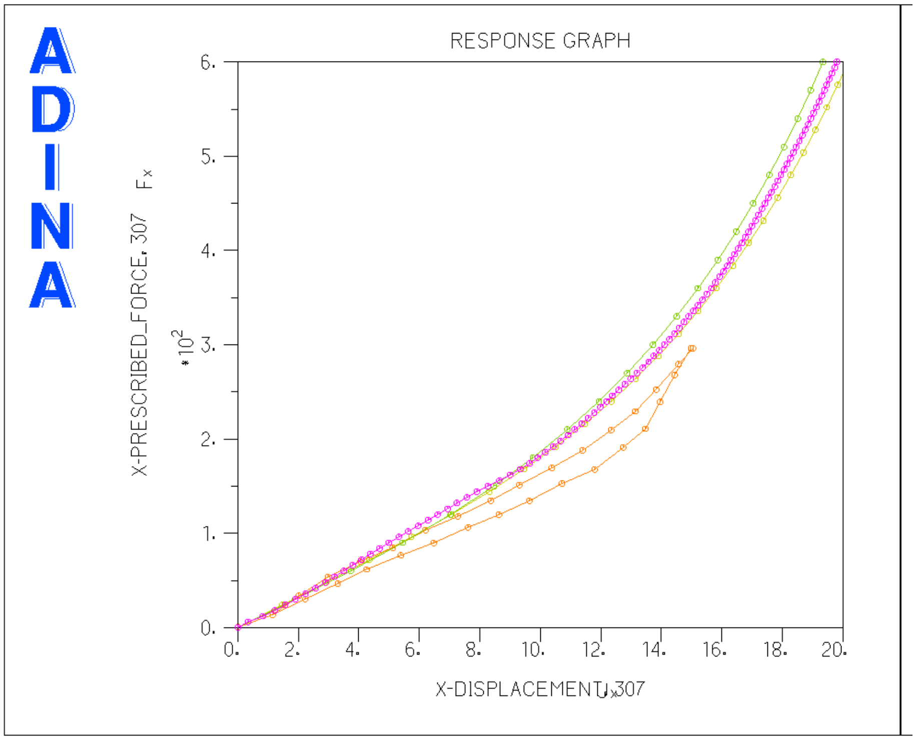

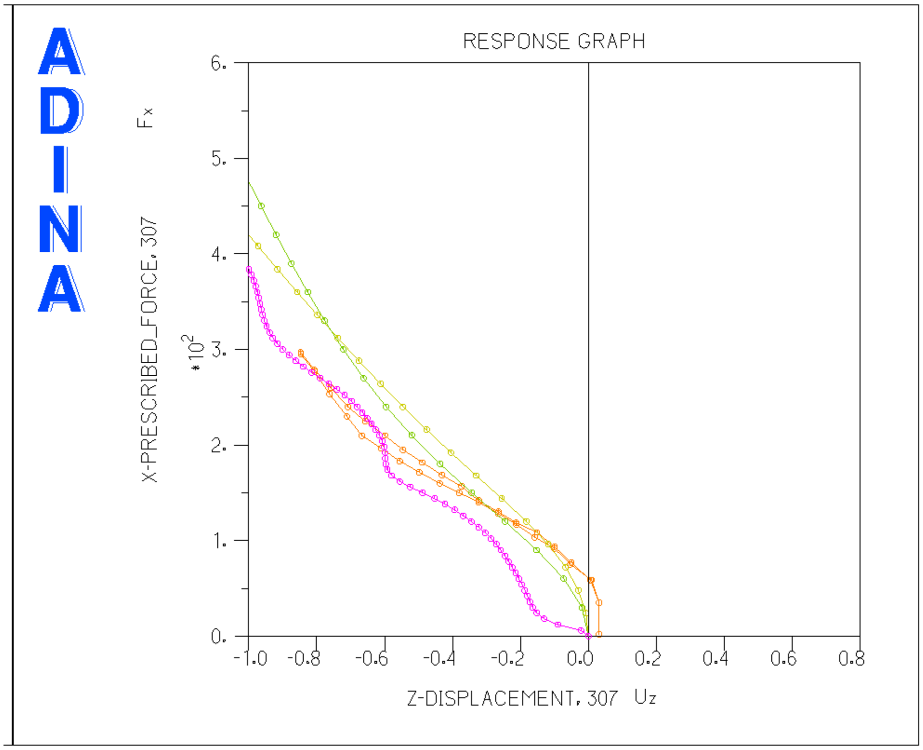

Figure 3.36 X-displacement (top) and z-displacement (bottom) with respect to the applied force
Ogden c-fit model: olive curve; Arruda-Boyce model: green curve;
Sussman-Bathe model: red curve; Experimental data: orange curve

It is observed that these three models predict similar x-displacement which is close to experimental data. For z-displacement, when the strain is relatively large, the Sussman-Bathe model will produce a better z-displacement simulation result. On the other hand, when the external force is small, the Ogden and Arruda-Boyce model achieve a better z-displacement simulation result.

3.2.3 Similar simulation with Treloar's experimental data

The same non-homogenous shear deformation simulations as described in chapter 3.2.1 were carried out for the material models built with Treloar's data in chapter 3.1. Although there is no experimental data available for non-homogenous shear deformation using the same rubber material as Treloar, the trend of deformation should be similar to P.A.J. van den Bogert and R. de. Borst's experimental results.

In addition to the Mooney-Rivlin model, Arruda-Boyce model and the Sussman-Bathe model, the Ogden model with constants given by Ogden[34] which produces good closeness to Treloar's pure shear data, is employed. The x-displacement and z-displacement simulation results are shown in figure 3.37.

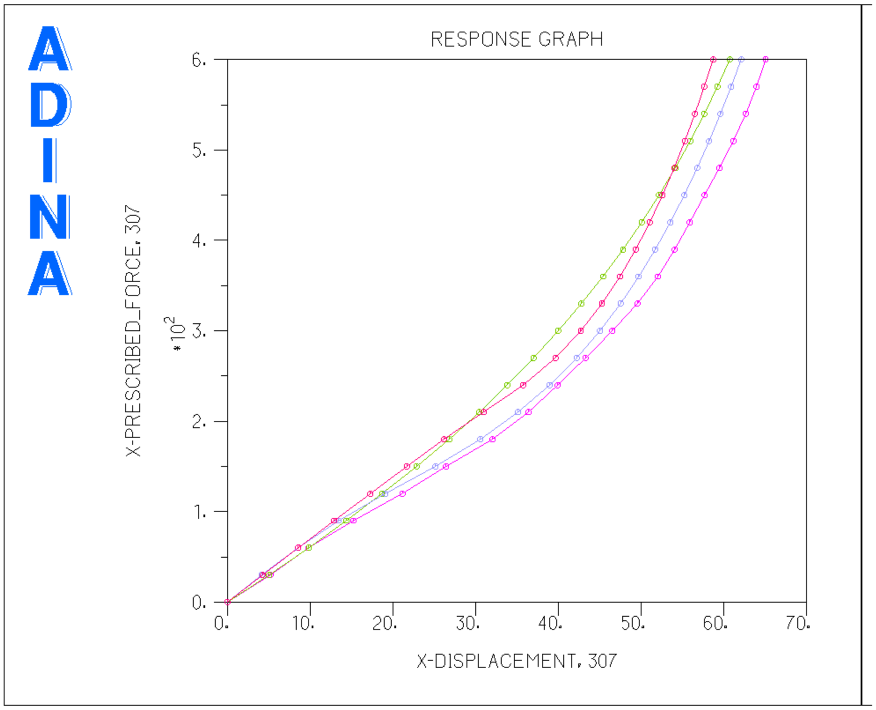

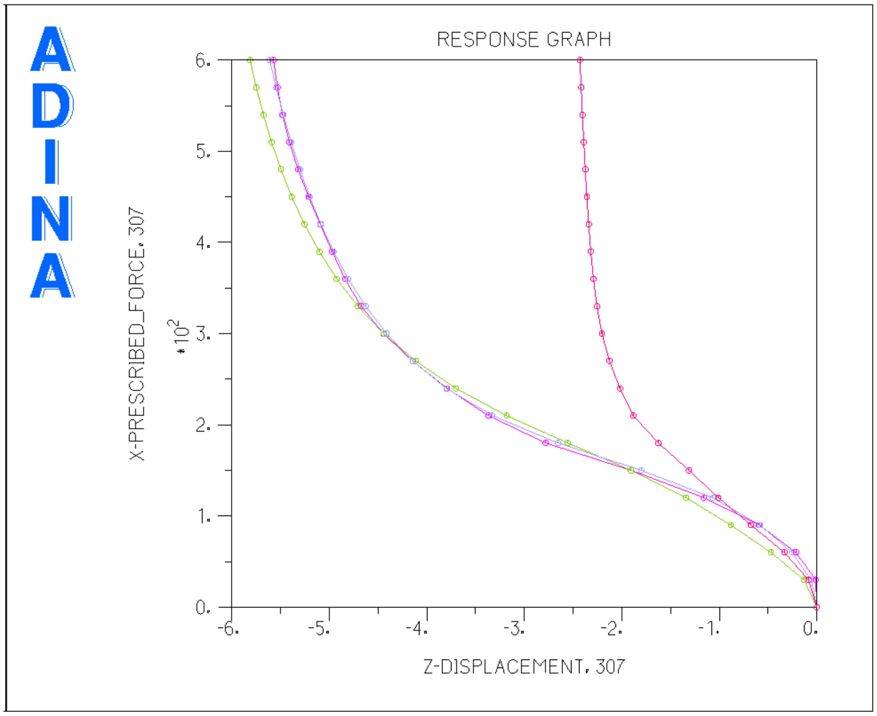

Figure 3.37 X-displacement (top) and z-displacement (bottom) with respect to the applied force
Mooney-Rivlin model: Red curve; Arruda-Boyce model: Olive curve;
Ogden model: blue curve; Sussman-Bathe model: Magenta curve

As shown in figure 3.37, the x-displacements of all four models are similar and have correct trend. Furthermore, negative z-displacement which is physically true is produced by all four models. It is important to note that not all the α s of the Ogden model are positive but it still predicts the correct z-displacement. Therefore, it cannot be simply concluded from chapter 3.2.2 that for Ogden model, it must have all positive α s to produce correct simulation results.

3.3 Conclusions

The predictive capability of various rubber material models is thoroughly studied in this chapter with pure shear numerical tests and non-homogenous shear numerical tests.

A good curve fitting of the material constants is difficult to obtain even with the convenient interface of ADINA. The newly-proposed Sussman-Bathe model for which no constants are needed is a significant shift in direction of studying strain energy density. Furthermore, the Sussman-Bathe model predicts the most accurate pure shear deformation curve based on uniaxial experimental data.

Both extension and compression data are required for rubber material model building. When only the uniaxial extension experimental data is given, there could be multiple good curve fits. For instance, the a-fit, b-fit and e-fit Ogden models all fit the extension experimental data well. However, for larger strain or compression deformation the difference of predicted stress-strain curves between these models becomes very large.

Even when the uniaxial experimental data is well fitted, the material model may not be able to predict the non-homogenous deformation correctly. For example, although the a-fit, b-fit and e-ft Ogden models all fit the uniaxial experimental data well, they are not able to attain reasonable z-displacement in the non-homogenous deformation numerical tests.

The performance of the Sussman-Bathe model depends on the data used to build the model. In the above research, the Sussman-Bathe model fitted from different Ogden models present different simulation results. When the c-fit Ogden model produces a physically correct z-displacement, the corresponding Sussman-Bathe model generates a similar physically correct z-displacement. On the other hand, when the Ogden models (a-fit or e-fit) can not produce reasonable results, neither could the corresponding Sussman-Bathe model.

Finally, all four models fitted with the Treloar's experimental data achieve reasonable simulation results for non-homogenous deformation.

Chapter 4

Stability of material models

4.1 Stability criterion deduction

4.1.1 Incremental deformation with respect to true strains

Consider a unit rubber cube under incompressible deformation, as shown in the figure 4.1.

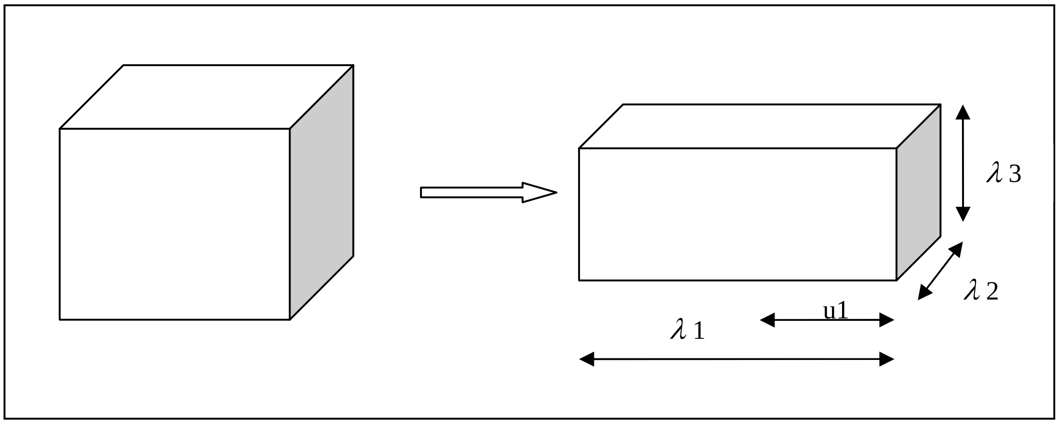

Figure 4.1 Unit cube under deformation

Assuming the strain energy density is expressed as $\varphi = \varphi(e_1, e_2, e_3)$, where e_1, e_2, e_3 are the true strains and related to the principal stretches and displacement as:

$$\begin{cases} e_i = \ln(\lambda_i) \\ \lambda_i = 1 + u_i \end{cases}. \tag{4.1}$$

where λ_i is the stretch in i direction and u_i is the displacement in i direction.

For incompressible rubber material, there is a constraint that its volume does not change during deformation. This means that $\lambda_1\lambda_2\lambda_3 = 1$ or $e_1 + e_2 + e_3 = 0$. Hence, to include this constraint into consideration, a Lagrange multiplier k is introduced and the strain energy density is modified as:

$$\hat{\varphi} = \varphi + k(e_1 + e_2 + e_3) \,. \tag{4.2}$$

There is no energy dissipation for elastic material. Therefore, the variation of strain energy is equal to the variation of work done by the external force: $\delta\hat{\varphi} = \delta R$, where R stands for the external work,

$$\begin{aligned} \delta\hat{\varphi} &= \sum_i \left(\frac{\partial\varphi}{\partial e_i} + k\right)\delta e_i + \delta k(e_1 + e_2 + e_3) \\ &= \sum_i \left(\frac{\partial\varphi}{\partial e_i} + k\right)\delta e_i \end{aligned} \tag{4.3}$$

$$\delta R = \sum_i R_i \delta u_i = \sum_i R_i \lambda_i \delta e_i \tag{4.4}$$

where R_i are the deformation independent loads per unit original area in i direction. Therefore, from $\delta\hat{\varphi} = \delta R$, we obtain that:

$$\sum_i \left(\frac{\partial\varphi}{\partial e_i} + k\right)\delta e_i = \sum_i R_i \lambda_i \delta e_i \tag{4.5}$$

(4.5) can be simplified to the equilibrium equations:

$$\begin{cases} \dfrac{\partial\varphi}{\partial e_i} + k = R_i \lambda_i \\ e_1 + e_2 + e_3 = 0 \end{cases} \tag{4.6}$$

Further, taking the variation of (4.6) with respect to e_1, e_2, e_3, we obtain that:

$$\begin{gathered} \begin{cases} \left(\dfrac{\partial^2\varphi}{\partial e_i \partial e_j}\right)\delta e_j + \delta k = \delta R_i \lambda_i + R_i \delta\lambda_i \\ e_1 + e_2 + e_3 = 0 \end{cases} \\ \Rightarrow \begin{cases} \sum_j \left(\dfrac{\partial^2\varphi}{\partial e_i \partial e_j}\right)\delta e_j - R_i \lambda_i \delta e_i + \delta k = \delta R_i \lambda_i \\ \delta e_1 + \delta e_2 + \delta e_3 = 0 \end{cases} \end{gathered} \tag{4.7}$$

Expressing the above equations in matrix form,

$$
\begin{bmatrix}
\frac{\partial^2\varphi}{\partial e_1\partial e_1}-e^{e_1}R_1 & \frac{\partial^2\varphi}{\partial e_1\partial e_2} & \frac{\partial^2\varphi}{\partial e_1\partial e_3} & 1 \\
\frac{\partial^2\varphi}{\partial e_2\partial e_1} & \frac{\partial^2\varphi}{\partial e_2\partial e_2}-e^{e_2}R_2 & \frac{\partial^2\varphi}{\partial e_2\partial e_3} & 1 \\
\frac{\partial^2\varphi}{\partial e_3\partial e_1} & \frac{\partial^2\varphi}{\partial e_3\partial e_2} & \frac{\partial^2\varphi}{\partial e_3\partial e_3}-e^{e_3}R_3 & 1 \\
1 & 1 & 1 & 0
\end{bmatrix}
\times
\begin{bmatrix}\Delta e_1\\ \Delta e_2\\ \Delta e_3\\ \Delta k\end{bmatrix}
=
\begin{bmatrix}e^{e_1}\Delta R_1\\ e^{e_2}\Delta R_2\\ e^{e_3}\Delta R_3\\ 0\end{bmatrix}
\tag{4.8}
$$

Using the Mooney-Rivlin model for instance, the strain energy density function is

$$
\begin{aligned}
\varphi &= c_1(I_1-3)+c_2(I_2-3)\\
&= c_1(\lambda_1^2+\lambda_2^2+\lambda_3^2-3)+c_2(\lambda_1^2\lambda_2^2+\lambda_2^2\lambda_3^2+\lambda_1^2\lambda_3^2-3)\\
&= c_1(e^{2e_1}+e^{2e_2}+e^{2e_3}-3)+c_2(e^{2e_1+2e_2}+e^{2e_2+2e_3}+e^{2e_1+2e_3}-3)
\end{aligned}
\tag{4.9}
$$

This leads to

$$
\begin{cases}
\frac{\partial\varphi}{\partial e_1}=2c_1\lambda_1^2+2c_2\lambda_1^2\lambda_2^2+2c_2\lambda_1^2\lambda_3^2\\
\frac{\partial\varphi}{\partial e_2}=2c_1\lambda_2^2+2c_2\lambda_1^2\lambda_2^2+2c_2\lambda_2^2\lambda_3^2\\
\frac{\partial\varphi}{\partial e_3}=2c_1\lambda_3^2+2c_2\lambda_1^2\lambda_3^2+2c_2\lambda_2^2\lambda_3^2
\end{cases}
\tag{4.10}
$$

and

$$
\begin{cases}
\frac{\partial^2\varphi}{\partial e_1\partial e_1}=4c_1\lambda_1^2+4c_2\lambda_1^2\lambda_2^2+4c_2\lambda_1^2\lambda_3^2\\
\frac{\partial^2\varphi}{\partial e_2\partial e_2}=4c_1\lambda_2^2+4c_2\lambda_1^2\lambda_2^2+4c_2\lambda_2^2\lambda_3^2\\
\frac{\partial^2\varphi}{\partial e_3\partial e_3}=4c_1\lambda_3^2+4c_2\lambda_3^2\lambda_2^2+4c_2\lambda_1^2\lambda_3^2\\
\frac{\partial^2\varphi}{\partial e_1\partial e_2}=4c_2\lambda_1^2\lambda_2^2\\
\frac{\partial^2\varphi}{\partial e_1\partial e_3}=4c_2\lambda_2^2\lambda_3^2\\
\frac{\partial^2\varphi}{\partial e_2\partial e_3}=4c_2\lambda_1^2\lambda_3^2
\end{cases}
\tag{4.11}
$$

Substituting equations (4.11) back to (4.8), the matrix can be simplified into

$$\begin{bmatrix} 4c_1\lambda_1^2+4c_2\lambda_1^2\lambda_2^2+4c_2\lambda_1^2\lambda_3^2-R_1\lambda_1 & 4c_2\lambda_1^2\lambda_2^2 & 4c_2\lambda_1^2\lambda_3^2 & 1 \\ 4c_2\lambda_1^2\lambda_2^2 & 4c_1\lambda_2^2+4c_2\lambda_1^2\lambda_2^2+4c_2\lambda_2^2\lambda_3^2-R_2\lambda_2 & 4c_2\lambda_2^2\lambda_3^2 & 1 \\ 4c_2\lambda_1^2\lambda_3^2 & 4c_2\lambda_2^2\lambda_3^2 & 4c_1\lambda_3^2+4c_2\lambda_1^2\lambda_3^2+4c_2\lambda_2^2\lambda_3^2-R_3\lambda_3 & 1 \\ 1 & 1 & 1 & 0 \end{bmatrix}$$

$$\times\begin{bmatrix}\Delta e_1\\ \Delta e_2\\ \Delta e_3\\ \Delta k\end{bmatrix}=\begin{bmatrix}e^{e_1}\Delta R_1\\ e^{e_2}\Delta R_2\\ e^{e_3}\Delta R_3\\ 0\end{bmatrix} \tag{4.12}$$

Substituting equation (4.10) back to (4.6),

$$\Rightarrow\begin{cases}2c_1\lambda_1^2+2c_2\lambda_1^2\lambda_2^2+2c_2\lambda_1^2\lambda_3^2+k=R_1\lambda_1\\ 2c_1\lambda_2^2+2c_2\lambda_1^2\lambda_2^2+2c_2\lambda_2^2\lambda_3^2+k=R_2\lambda_2\\ 2c_1\lambda_3^2+2c_2\lambda_1^2\lambda_3^2+2c_2\lambda_2^2\lambda_3^2+k=R_3\lambda_3\end{cases} \tag{4.13}$$

(1) Uniaxial deformation

Substituting

$$\begin{cases}R_2=R_3=0\\ e_2=e_3=-\dfrac{e_1}{2}\end{cases}$$

into equation (4.12),

$$\begin{bmatrix} 4c_1\lambda_1^2+8c_2\lambda_1-R_1\lambda_1 & 4c_2\lambda_1 & 4c_2\lambda_1 & 1 \\ 4c_2\lambda_1 & 4c_1\lambda_1^{-1}+4c_2\lambda_1^{-2}+4c_2\lambda_1 & 4c_2\lambda_1^{-2} & 1 \\ 4c_2\lambda_1 & 4c_2\lambda_1^{-2} & 4c_1\lambda_1^{-1}+4c_2\lambda_1^{-2}+4c_2\lambda_1 & 1 \\ 1 & 1 & 1 & 0 \end{bmatrix}\times\begin{bmatrix}\Delta e_1\\ \Delta e_2\\ \Delta e_3\\ \Delta k\end{bmatrix}=\begin{bmatrix}e^{e_1}\Delta R_1\\ 0\\ 0\\ 0\end{bmatrix} \tag{4.14}$$

Substitute $R_2=R_3=0$ into equation (4.13), the equilibrium equations (4.6) become:

$$\begin{cases}2c_1\lambda_1^2+2c_2\lambda_1^2\lambda_2^2+2c_2\lambda_1^2\lambda_3^2+k=R_1\lambda_1\\ 2c_1\lambda_2^2+2c_2\lambda_1^2\lambda_2^2+2c_2\lambda_2^2\lambda_3^2+k=R_2\lambda_2=0\\ 2c_1\lambda_3^2+2c_2\lambda_1^2\lambda_3^2+2c_2\lambda_2^2\lambda_3^2+k=R_3\lambda_3=0\\ \lambda_2=\lambda_3=\lambda_1^{-1/2}\end{cases}$$

$$\Rightarrow 2c_1\lambda_1^2+2c_2\lambda_1-2c_1\lambda_1^{-1}-2c_2\lambda_1^{-2}=R_1\lambda_1$$

$$\Rightarrow R_1=2c_1\lambda_1+2c_2-2c_1\lambda_1^{-2}-2c_2\lambda_1^{-3} \tag{4.15}$$

Substituting R_1 into equation (4.14), the stability matrix is obtained:

$$
\begin{bmatrix}
2c_1\lambda_1^2 + 6c_2\lambda_1 + 2c_1\lambda_1^{-1} + 2c_2\lambda_1^{-2} & 4c_2\lambda_1 & 4c_2\lambda_1 & 1 \\
4c_2\lambda_1 & 4c_1\lambda_1^{-1} + 4c_2\lambda_1^{-2} + 4c_2\lambda_1 & 4c_2\lambda_1^{-2} & 1 \\
4c_2\lambda_1 & 4c_2\lambda_1^{-2} & 4c_1\lambda_1^{-1} + 4c_2\lambda_1^{-2} + 4c_2\lambda_1 & 1 \\
1 & 1 & 1 & 0
\end{bmatrix}
$$

(2) Biaxial deformation

Substituting

$$
\begin{cases}
R_1 = R_2 \\
R_3 = 0 \\
e_1 = e_2 \\
e_3 = -2e_1
\end{cases}
$$

into equation (4.12),

$$
\begin{bmatrix}
4c_1\lambda_1^2 + 4c_2\lambda_1^4 + 4c_2\lambda_1^{-2} - R_1\lambda_1 & 4c_2\lambda_1^4 & 4c_2\lambda_1^{-2} & 1 \\
4c_2\lambda_1^4 & 4c_1\lambda_1^2 + 4c_2\lambda_1^4 + 4c_2\lambda_1^{-2} - R_1\lambda_1 & 4c_2\lambda_1^{-2} & 1 \\
4c_2\lambda_1^{-2} & 4c_2\lambda_1^{-2} & 4c_1\lambda_1^{-4} + 8c_2\lambda_1^{-2} & 1 \\
1 & 1 & 1 & 0
\end{bmatrix}
$$

$$
\times \begin{bmatrix} \Delta e_1 \\ \Delta e_2 \\ \Delta e_3 \\ \Delta k \end{bmatrix} = \begin{bmatrix} e^{e_1}\Delta R_1 \\ e^{e_2}\Delta R_2 \\ e^{e_3}\Delta R_3 \\ 0 \end{bmatrix} \tag{4.16}
$$

Substituting

$$
\begin{cases}
R_1 = R_2 \\
R_3 = 0
\end{cases}
$$

into equation (4.13), the equilibrium equation becomes

$$
\begin{cases}
2c_1\lambda_1^2 + 2c_2\lambda_1^2\lambda_2^2 + 2c_2\lambda_1^2\lambda_3^2 + k = R_1\lambda_1 \\
2c_1\lambda_2^2 + 2c_2\lambda_1^2\lambda_2^2 + 2c_2\lambda_2^2\lambda_3^2 + k = R_2\lambda_2 \\
2c_1\lambda_3^2 + 2c_2\lambda_1^2\lambda_3^2 + 2c_2\lambda_2^2\lambda_3^2 + k = R_3\lambda_3 = 0 \\
\lambda_1 = \lambda_2 \\
\lambda_3 = \lambda_1^{-2}
\end{cases}
$$

$$
\Rightarrow 2c_1\lambda_1^2 + 2c_2\lambda_1^4 - 2c_2\lambda_1^{-2} - 2c_1\lambda_1^{-4} = R_1\lambda_1 \tag{4.17}
$$

Substitute R_1 into equation (4.16), the stability matrix becomes

$$\begin{bmatrix} 2c_1\lambda_1^2+2c_2\lambda_1^4+6c_2\lambda_1^{-2}+2c_1\lambda_1^{-4} & 4c_2\lambda_1^4 & 4c_2\lambda_1^{-2} & 1 \\ 4c_2\lambda_1^4 & 2c_1\lambda_1^2+2c_2\lambda_1^4+6c_2\lambda_1^{-2}+2c_1\lambda_1^{-4} & 4c_2\lambda_1^{-2} & 1 \\ 4c_2\lambda_1^{-2} & 4c_2\lambda_1^{-2} & 4c_1\lambda_1^{-4}+8c_2\lambda_1^{-2} & 1 \\ 1 & 1 & 1 & 0 \end{bmatrix}$$

(3) Pure Shear deformation

Substituting

$$\begin{cases} R_3=0 \\ e_2=0 \\ e_3=-e_1 \end{cases}$$

into equation (4.12),

$$\begin{bmatrix} 4c_1\lambda_1^2+4c_2\lambda_1^2+4c_2-R_1\lambda_1 & 4c_2\lambda_1^2 & 4c_2 & 1 \\ 4c_2\lambda_1^2 & 4c_1+4c_2\lambda_1^2+4c_2\lambda_1^{-2}-R_2 & 4c_2\lambda_1^{-2} & 1 \\ 4c_2 & 4c_2\lambda_1^{-2} & 4c_1\lambda_1^{-2}+4c_2\lambda_1^{-2}+4c_2 & 1 \\ 1 & 1 & 1 & 0 \end{bmatrix}$$
$$\times\begin{bmatrix} \Delta e_1 \\ \Delta e_2 \\ \Delta e_3 \\ \Delta k \end{bmatrix}=\begin{bmatrix} e^{e_1}\Delta R_1 \\ e^{e_2}\Delta R_2 \\ 0 \\ 0 \end{bmatrix} \tag{4-18}$$

Substituting

$$\begin{cases} R_3=0 \\ e_2=0 \\ e_3=-e_1 \end{cases}$$

into equation (4.13), the equilibrium equation becomes

$$\begin{cases} 2c_1\lambda_1^2+2c_2\lambda_1^2\lambda_2^2+2c_2\lambda_1^2\lambda_3^2+k=R_1\lambda_1 \\ 2c_1\lambda_2^2+2c_2\lambda_1^2\lambda_2^2+2c_2\lambda_2^2\lambda_3^2+k=R_2\lambda_2 \\ 2c_1\lambda_3^2+2c_2\lambda_1^2\lambda_3^2+2c_2\lambda_2^2\lambda_3^2+k=R_3\lambda_3=0 \\ \lambda_2=1 \\ \lambda_3=\lambda_1^{-1} \end{cases}$$

$$\Rightarrow \begin{cases} 2c_1\lambda_1^2 + 2c_2\lambda_1^2 - 2c_1\lambda_1^{-2} - 2c_2\lambda_1^{-2} = R_1\lambda_1 \\ 2c_1 + 2c_2\lambda_1^2 - 2c_1\lambda_1^{-2} - 2c_2 = R_2\lambda_2 \end{cases} \tag{4.19}$$

Substituting R_1 and R_2 into equation (4.18), the stability matrix obtained is

$$\begin{bmatrix} 2c_1\lambda_1^2 + 2c_2\lambda_1^2 + 4c_2 + 2c_1\lambda_1^{-2} + 2c_2\lambda_1^{-2} & 4c_2\lambda_1^2 & 4c_2 & 1 \\ 4c_2\lambda_1^2 & 2c_1 + 2c_2\lambda_1^2 + 4c_2\lambda_1^{-2} + 2c_1\lambda_1^{-2} + 2c_2 & 4c_2\lambda_1^{-2} & 1 \\ 4c_2 & 4c_2\lambda_1^{-2} & 4c_1\lambda_1^{-2} + 4c_2\lambda_1^{-2} + 4c_2 & 1 \\ 1 & 1 & 1 & 0 \end{bmatrix}$$

4.1.2 Stability analysis

Based on the above analysis of incremental deformation, the incremental formula can be generalized as

$$\begin{bmatrix} K_{11} & K_{12} & K_{13} & 1 \\ K_{21} & K_{22} & K_{23} & 1 \\ K_{31} & K_{32} & K_{33} & 1 \\ 1 & 1 & 1 & 0 \end{bmatrix} \times \begin{bmatrix} \Delta e_1 \\ \Delta e_2 \\ \Delta e_3 \\ \Delta k \end{bmatrix} = \begin{bmatrix} e^{e_1}\Delta R_1 \\ e^{e_2}\Delta R_2 \\ e^{e_3}\Delta R_3 \\ 0 \end{bmatrix} \tag{4.20}$$

where component of stability matrix K_{ij} varies with different rubber material models and different deformation types. If a rubber material is stable, then physically the external work, which is

$$\Delta u_i \Delta R_i = e^{e_1}\Delta e_i \Delta R_i = \begin{bmatrix} \Delta e_1 & \Delta e_2 & \Delta e_3 \end{bmatrix} \bullet \begin{bmatrix} e^{e_1}\Delta R_1 \\ e^{e_2}\Delta R_2 \\ e^{e_3}\Delta R_3 \end{bmatrix} = \begin{bmatrix} \Delta e_1 & \Delta e_2 & \Delta e_3 & \Delta k \end{bmatrix} \bullet \begin{bmatrix} e^{e_1}\Delta R_1 \\ e^{e_2}\Delta R_2 \\ e^{e_3}\Delta R_3 \\ 0 \end{bmatrix} \tag{4.21}$$

should always be positive. The external work is equal to the right hand side of equation (4.20) multiplied by $\begin{bmatrix} \Delta e_1 & \Delta e_2 & \Delta e_3 & \Delta k \end{bmatrix}$ as shown in equation (4.21). Hence, the left hand side of equation (4.10) multiplied by $\begin{bmatrix} \Delta e_1 & \Delta e_2 & \Delta e_3 & \Delta k \end{bmatrix}$, should also always be positive as shown in (4.22)

$$\begin{bmatrix}\Delta e_1 & \Delta e_2 & \Delta e_3 & \Delta k\end{bmatrix}\bullet\begin{bmatrix}K_{11} & K_{12} & K_{13} & 1\\ K_{21} & K_{22} & K_{23} & 1\\ K_{31} & K_{32} & K_{33} & 1\\ 1 & 1 & 1 & 0\end{bmatrix}\bullet\begin{bmatrix}\Delta e_1\\ \Delta e_2\\ \Delta e_3\\ \Delta k\end{bmatrix} = \Delta u_i \Delta R_i > 0 \tag{4.22}$$

Hence, from the definition of positive definite matrix, the above 4 by 4 matrix should be positive definite if $\begin{bmatrix}\Delta e_1 & \Delta e_2 & \Delta e_3 & \Delta k\end{bmatrix}$ is independent. However, from the constraint of incompressibility, there is a constraint for $\Delta e_1, \Delta e_2, \Delta e_3$ requiring that $\Delta e_1 + \Delta e_2 + \Delta e_3 = 0$, which implies that $\Delta e_1, \Delta e_2, \Delta e_3$ are not independent. This constraint needs to impose on the above 4 by 4 matrix to ensure that equation (4.22) is always positive.

With $\Delta e_1 + \Delta e_2 + \Delta e_3 = 0$, we have hat $\Delta e_1 = -\Delta e_2 - \Delta e_3$, which then is substituted into equation (4.22)

$$\begin{aligned}
&\begin{bmatrix}\Delta e_1 & \Delta e_2 & \Delta e_3 & \Delta k\end{bmatrix}\bullet\begin{bmatrix}K_{11} & K_{12} & K_{13} & 1\\ K_{21} & K_{22} & K_{23} & 1\\ K_{31} & K_{32} & K_{33} & 1\\ 1 & 1 & 1 & 0\end{bmatrix}\bullet\begin{bmatrix}\Delta e_1\\ \Delta e_2\\ \Delta e_3\\ \Delta k\end{bmatrix}\\
&= \begin{bmatrix}\Delta e_1 & \Delta e_2 & (-\Delta e_1 - \Delta e_2) & \Delta k\end{bmatrix}\bullet\begin{bmatrix}K_{11} & K_{12} & K_{13} & 1\\ K_{21} & K_{22} & K_{23} & 1\\ K_{31} & K_{32} & K_{33} & 1\\ 1 & 1 & 1 & 0\end{bmatrix}\bullet\begin{bmatrix}\Delta e_1\\ \Delta e_2\\ (-\Delta e_1 - \Delta e_2)\\ \Delta k\end{bmatrix}\\
&= \begin{bmatrix}\Delta e_1 & \Delta e_2\end{bmatrix}\bullet\begin{bmatrix}K_{11} + K_{33} - 2K_{13} & K_{12} + K_{33} - K_{23} - K_{13}\\ K_{21} + K_{33} - K_{23} - K_{13} & K_{22} + K_{33} - 2K_{23}\end{bmatrix}\bullet\begin{bmatrix}\Delta e_1\\ \Delta e_2\end{bmatrix}
\end{aligned} \tag{4.23}$$

Therefore, to make equation (4.22) positive, the above 2 by 2 matrix in equation (4.23) must be positive definite, which means that its eigenvalues are always positive. For pure shear deformation, there is no strain in y-direction: $\Delta e_2 = 0$. Hence, the stability matrix is simplified to a 1 by 1 matrix.

Thus the stability matrix could be expressed in terms of true strain e, so are its eigenvalues. With the plot of eigenvalues with respect to true strain e, the stability of material model could be clearly shown. If the eigenvalues of a certain type of deformation are always positive throughout the entire strain range, then the material model will always be stable for this kind of deformation. Otherwise if the eigenvalue becomes negative at certain strain e, the material will be become unstable at that strain. Only if eigenvalues of all three deformations: uniaxial, biaxial and pure shear are always positive, the material model is regarded as always stable.

4.2 Stability criterion verification

4.2.1 Stability curves verification with different material models

A 2D model with a four node plane stress element is built in ADINA as shown in figure 4.2. The z-translation of line $L4$ and the y-translation of line $L1$ are fixed. The y-translation of line $L3$ and the z-translation of line $L2$ are constrained to the upper-right corner point $P3$ where the force is applied.

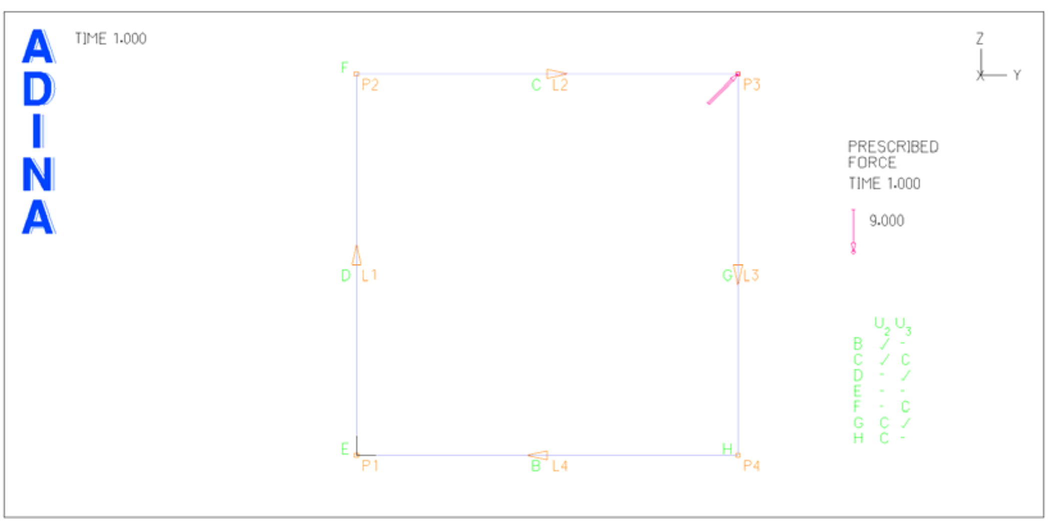

Figure 4.2 4-node plane stress model in ADINA

(1) Mooney-Rivlin model with constants $C_1 = 1$ and $C_2 = 1$

In upper part of figure 4.3, the stability curves show that the uniaxial and shear deformations are always stable while the biaxial deformation becomes unstable when the strain gets large. Low part of figure 4.3 shows clearly that the criterion point where the material becomes unstable is approximately 0.33.

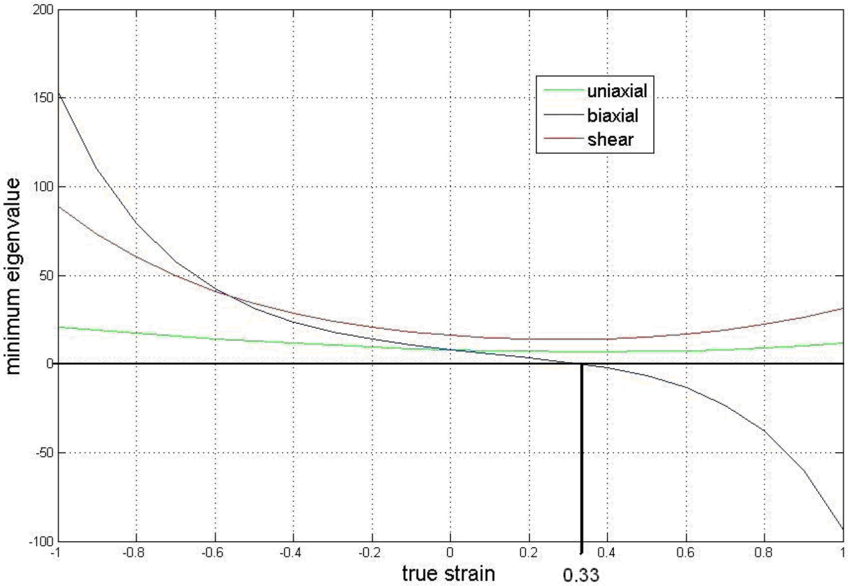

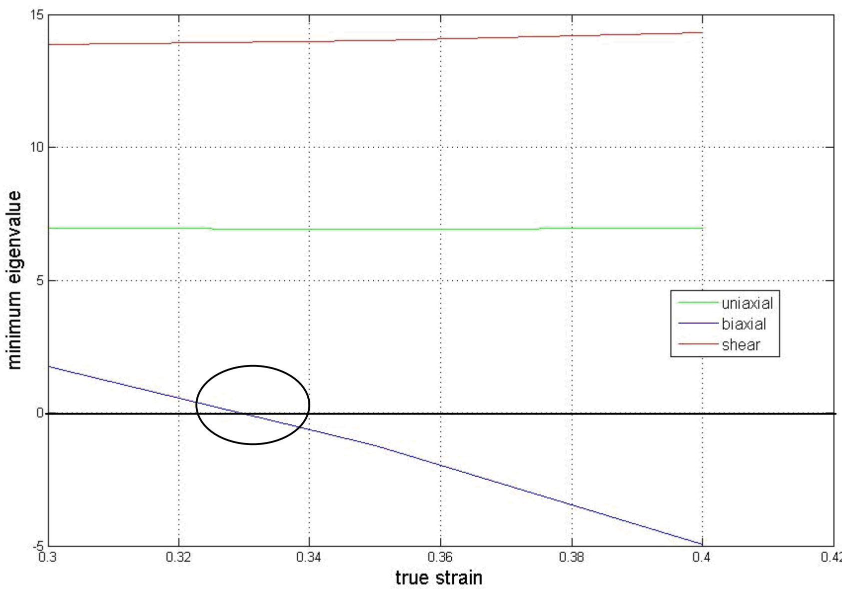

Figure 4.3 Stability curves with C_1 =1 and C_2 =1 by matlab (upper part: entire strain range; lower part: strain near criterion point)

Compared with the newly-available stability curves in ADINA, the eigenvalues calculated from Matlab have different values but have same signs, which are more important and determine the stability of material models. In fact, the criterion points are both 0.33 as shown in figure 4.3 and 4.4, which further illustrates the correctness of the re-derived stability criterion.

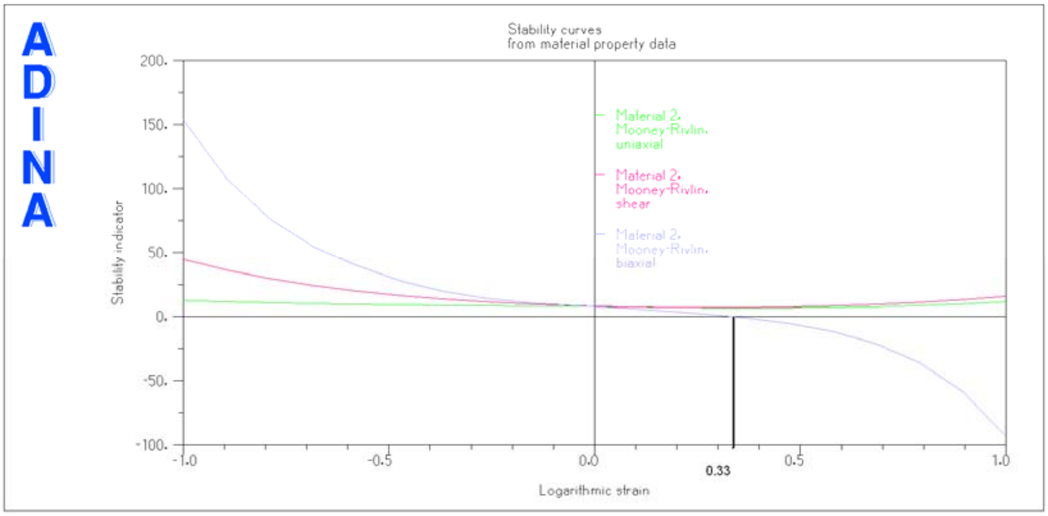

Figure 4.4 Stability curves with C_1=1 and C_2=1 by ADINA

(a) Test 1

When a biaxial force with a magnitude of 9.5N is applied on point P_3, the whole element undergoes homogenous deformation and results are shown in table 4.1:

Table 4.1 Results of test 1 (biaxial)

	YY	**ZZ**	**XX**
Engineering Strain	0.372	0.372	.0.4685
Engineering Stress	9.214 N/m^2	9.214 N/m^2	0 N/m^2

The corresponding true strain in Y direction is:

$$e = \ln(\lambda) = \ln(1.372) = 0.316$$

The material model is still within the stable range and a correct result is achieved. However, the strain is fairly close to the criterion value (0.33). If the force is further increased, there is the possibility that the material will become unstable.

(b) Test 2

When a biaxial force with a magnitude of 11 N is applied on point P_3 with 100 time steps, ADINA reports*"stiffness matrix not positive definite, boundary conditions or model collapsed and the grogram stops abnormally"*. In the output file, an error message in the 91st time step is found as shown below:

**** STIFFNESS MATRIX NOT POSITIVE DEFINITE ****
NODE=4 EQUATION=2   DOF= Z-translation   PIVOT= .3.74084103E.02

The largest true strain achieved by the above test is 0.3284 which coincides with the stability criterion predicted by the biaxial deformation stability curve.

(c) Test 3

When a uniaxial force with a magnitude of 100 N is applied on point P_3, the results are shown in table 4.2. It can be seen that even though the strain becomes very large, the uniaxial deformation is still stable, which is consistent with the prediction of the uniaxial deformation stability curve.

Table 4.2 Results of test 3 (uniaxial)

	YY	**ZZ**	**XX**
Engineering Strain	48	0.1429	0.8571
Engineering Stress	4900N/m^2	0 N/m^2	0 N/m^2

(d) Test 4

When a pure shear force with a magnitude of 100N was applied on point P_3, the results produced are summarized in table 4.3. When the strain becomes very large, the pure shear deformation is still stable, which is consistent with the prediction of the uniaxial deformation stability curve.

Table 4.3 Results of test 4 (pure shear)

	YY	ZZ	XX
Engineering Strain	24	0	.0.96
Engineering Stress	2500N/m^2	1250N/m^2	1250N/m^2

(2) Mooney-Rivlin model built with Treloar's data

The Mooney-Rivlin model is built as described in chapter 3.1 and the corresponding stability curves are shown in figure 4.5. It seems that it is stable for all three types of deformations. However, if the strain range is enlarged as shown in figure 4.6, the biaxial deformation will become unstable.

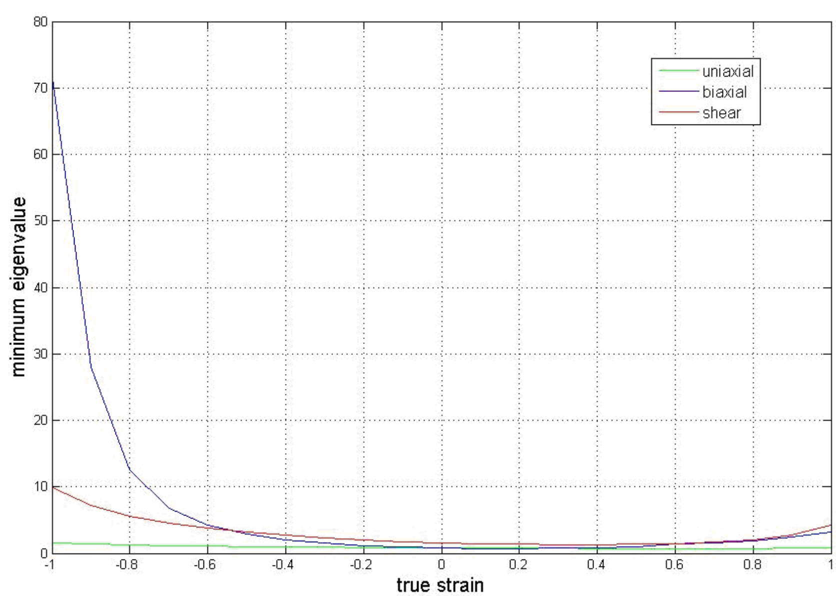

Figure 4.5 Stability curves of Mooney-Rivlin model built with Treloar's data

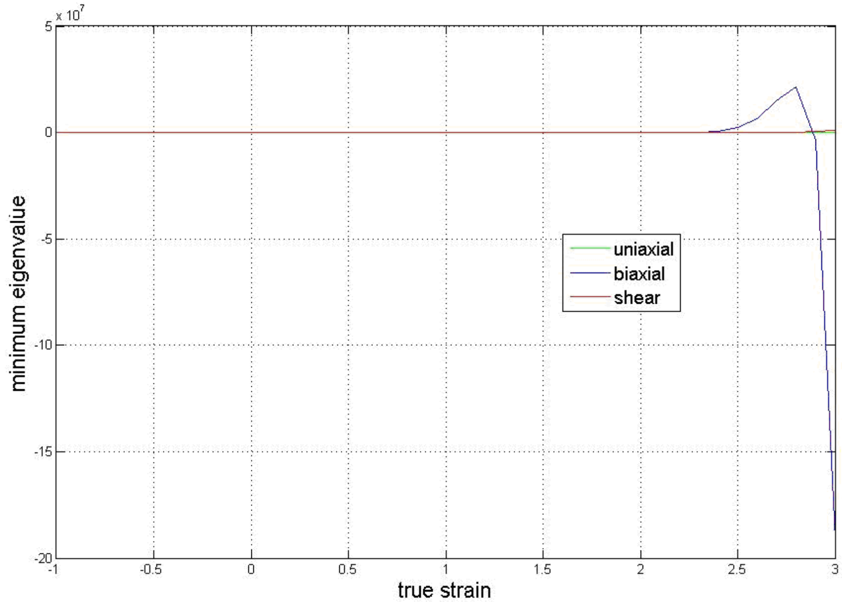

Figure 4.6 Stability curves of Mooney-Rivlin model built with Treloar's data (enlarged range)

As predicted by the stability curves, this material model is quite stable for uniaxial and shear deformation. Even when the loading is increased to 100N, resulting in a stretch ratio of around 14, correct results can still be achieved. The corresponding results are summarized in table 4.4.

Table 4.4 Results of uniaxial test with Mooney-Rivlin model

	force	stress	Stretch XX	Stretch YY	Stretch ZZ	J
MR model uniaxial	100	1472	0.2607	14.72	0.2607	1.000437

However it is clearly shown from figure 4.6 that for biaxial deformation, when the strain is relatively large (true strain $e > 2.8$), the material model becomes unstable. In addition, the ADINA numerical experiment proves this prediction as well. When a large force is applied in biaxial directions, the material becomes unstable and the simulation can not converge.

(3) Ogden model built with Treloar data

With Ogden's constant, the stability curve is shown in figure 4.7. All three deformations of this material model are always stable, even when the loading is increased to 100N which results in a stretch ratio around 15. Some test results are shown in table 4.5.

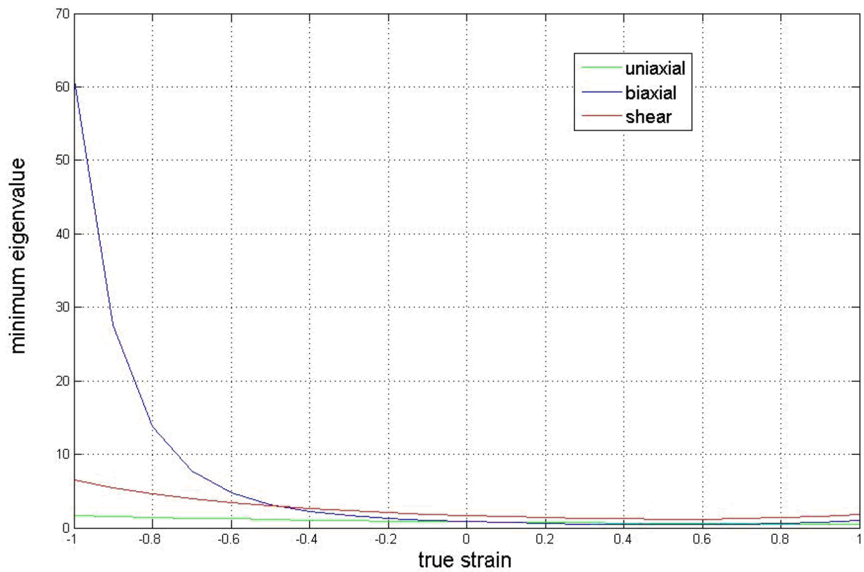

Figure 4.7 Stability curves of Ogden model built with Treloar's data

Table 4.5 Results of uniaxial and biaxial tests with Ogden model

	stress	Stretch XX	Stretch YY	Stretch ZZ	J
Uniaxial test	1678	0.2441	16.78	0.2441	0.999833
Biaxial test	1511	0.00438	15.11	15.11	1.000007

(4) Arruda-Boyce model with Treloar data

The stability curve of the Arruda-Boyce model is shown in figure 4.8. All three deformations of this material model are always stable, even when the loading is increased to 100N which results in a stretch ratio around 12. Some test results are shown in table 4.6.

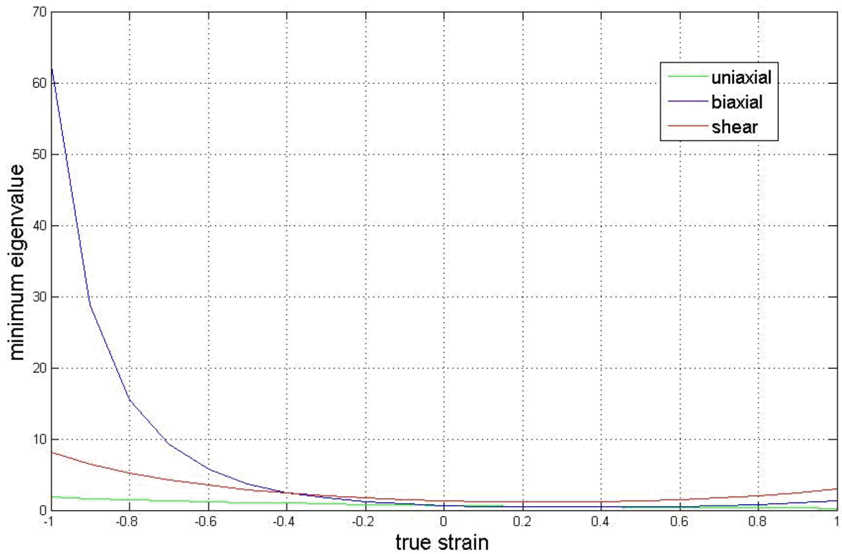

Figure 4.8 Stability curves of Arruda-Boyce model built with Treloar's data

Table 4.6 Results of uniaxial and biaxial tests with Arruda-Boyce model

	stress	Stretch XX	Stretch YY	Stretch ZZ	J
Uniaxial test	1289	0.2785	12.89	0.2785	0.999777
Biaxial test	954.8	0.01097	9.548	9.548	1.000072

(5) Sussman-Bathe model with Treloar data

As discussed earlier, the Sussman-Bathe model produces the most accurate material stress-strain relationship with given experimental data. Its stability curves are shown in figure 4.9. All three deformations of this material are always stable, even when the loading is increased to 100N which results in a stretch ratio around 10. Some test results are listed in table 4.7.

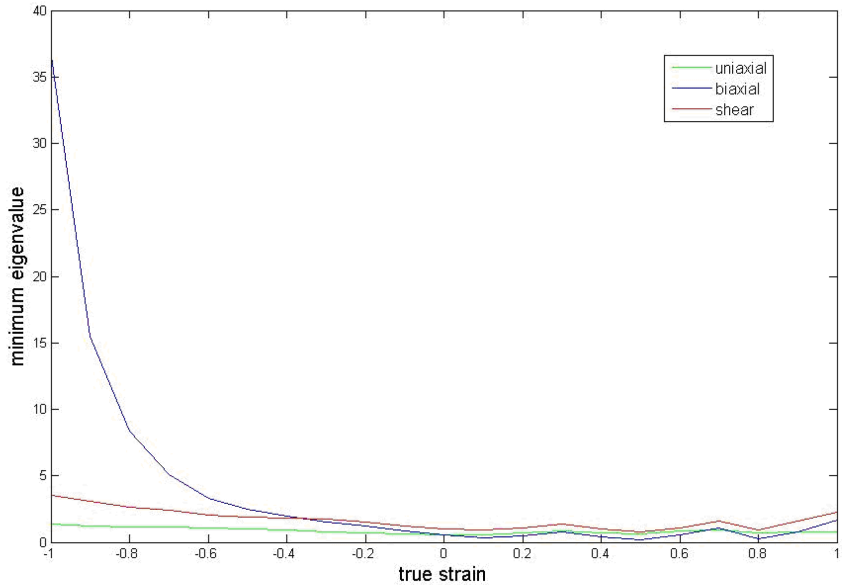

Figure 4.9 Stability curves of Sussman-Bathe model built with Treloar's data

Table 4.7 Results of uniaxial and biaxial tests with Sussman-Bathe model

	stress	**Stretch XX**	**Stretch YY**	**Stretch ZZ**	**J**
Uniaxial test	1017	0.3135	10.17	0.3135	0.99953
Biaxial test	1008	0.00985	10.08	10.08	1.000823

(6) Stability curve discussion

From the above numerical tests, it is observed that the stability curve is quite accurate. If the stability curve is positive, the corresponding deformation is stable and vice versa.

Using different methods to deal with the incompressibility constraint during the calculation of the stability matrix can result in different stability curves. For instance, at the step of imposing the incompressibility constraint (formula 4.23), the incremental true strain e_3 can be eliminated while reserving e_1 and e_2. On the other hand, the incremental true strain e_1 can be eliminated while keeping e_2 and e_3. This minor change will induce different final stability matrices and consequently different eigenvalues. However, the stability curve trends and signs of the eigenvalues are always the same. For example, if e_1 instead of e_3 is eliminated, the result for the Mooney-Rivlin model with C_1=1 and C_2=1 is shown in figure 4.10 as follows.

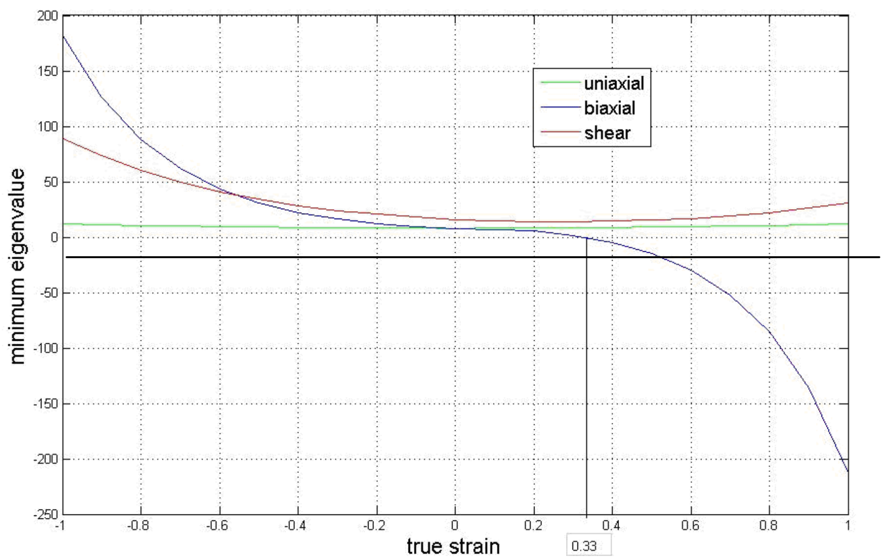

Figure 4.10 Stability curves with C_1=1 and C_2=1 (e_1 eliminated)

Comparing figure 4.10 with figure 4.5 and figure 4.6, these three figures are not completely the same but the curve trends are similar and most importantly, the signs of eigenvalues are all the same. Thus they all have the same criterion value 0.33.

If the matrix basis is changed to a new orthogonal set, the eigenvalues will not change. However, changing to a new independent but not orthogonal basis (for example, changing from "e_1, e_2, e_3" to "e_1, e_2, $e_1+e_2+e_3$") will change the eigenvalues of a matrix, although the signs of eigenvalues, and consequently the criterion value will not change. In fact different matrices can stand for same stability criterion. Giving a simple example, if matrix A is positive definite, $a*A$ (let “a” be a positive scalar) is also positive definite. The eigenvalues of A and $a*A$ are different but their signs remain the same. Thus, both matrix A and matrix $a*A$ can present the stability of a material model correctly.

Hence, different stability matrices can be derived using different methods. However, the signs of their eigenvalues will always be same.

4.2.2 Stability analysis of the non-homogenous shear deformations

(1) Models using Treloar’s data

From the above stability curve analysis, the four models fitted from the Treloar data in chapter 3.1 are all always stable, except for the biaxial deformation of the Mooney-Rivlin model. Correspondingly, above four models all produce physically reasonable x-displacement and z-displacement during the non-homogenous deformation as shown in chapter 3.2.3. On the other hand, the value of z-displacement predicted by the Mooney-Rivlin model is significantly different from the other three models as shown in figure 3.37.

(2) Mooney-Rivlin model using P.A.J. van den Bogert and R. de. Borst’s data

In chapter 3.2.1, two relatively accurate curve fittings by the Mooney-Rivlin model were discussed. One was directly fitted through ADINA by the Gaussian Elimination least square method (material model no.1), while the other was suggested by P.A.J.

van den Bogert and R. de. Borst (material model no.2). Corresponding to the physically impossible stress-strain curve produced by material model no.1 in figure 3.23, the stability curves of the three deformations are all negative as shown in figure 4.11.

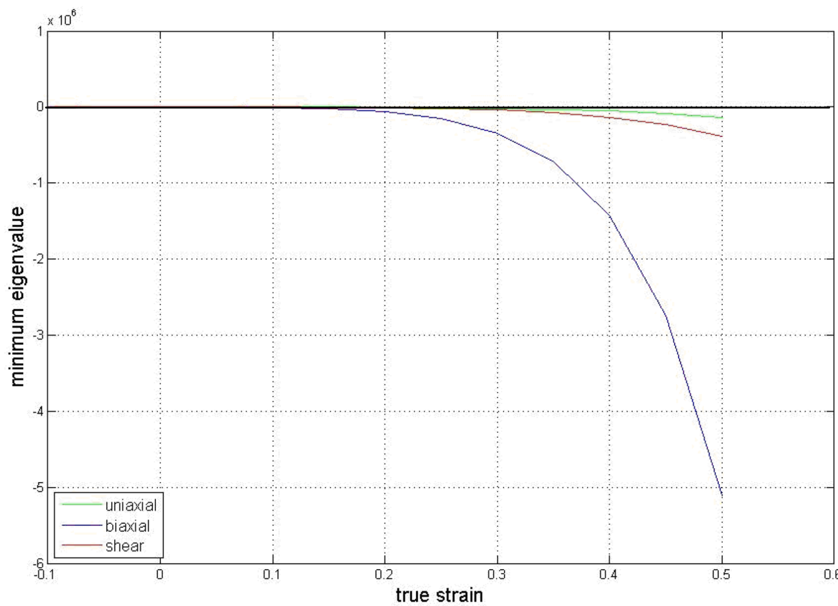

Figure 4.11 Stability curves of Mooney-Rivlin model with constants fitted by ADINA

On the other hand, for the P.A.J. van den Bogert and R. de. Borst's Mooney-Rivlin model, the uniaxial and shear deformations are always stable as shown in figure 4.12, although its biaxial deformation is still unstable, which is a limitation experienced by all Mooney-Rivlin models with 2 constants. Although there is no explicit biaxial deformation during the non-homogenous deformation tests, the simulation results of non-homogenous deformation is affected by the biaxial instability. Hence, as expected, the Mooney-Rivlin model no. 2 also does not produce a correct z-displacement at the beginning of deformation and generate a much larger z-displacement compared with experimental data as shown in figure 3.32.

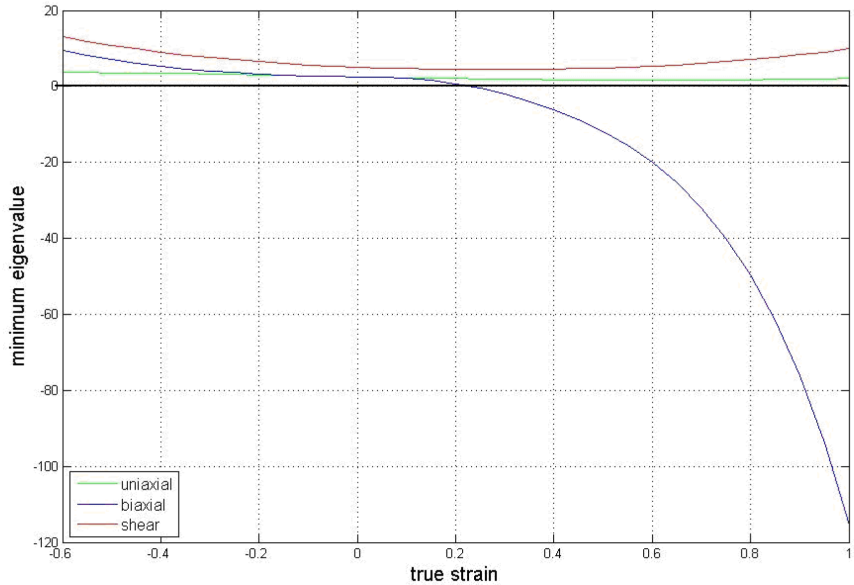

Figure 4.12 Stability curves of Mooney-Rivlin model with P.A.J. van den Bogert and R. de. Borst's constants

(3) Ogden model using P.A.J. van den Bogert and R. de. Borst's data

Four Ogden models (a-fit, b-fit, e-fit, ADINA-fit) are unstable for biaxial deformation as shown in figure 4.13, 4.14, 4.16 and 4.17. As expected, they produce physically unreasonable positive z-displacement as shown in chapter 3.2. On the other hand, the c-fit Ogden model, which is always stable as shown in figure 4.15, attains a negative z-displacement which is physically correct.

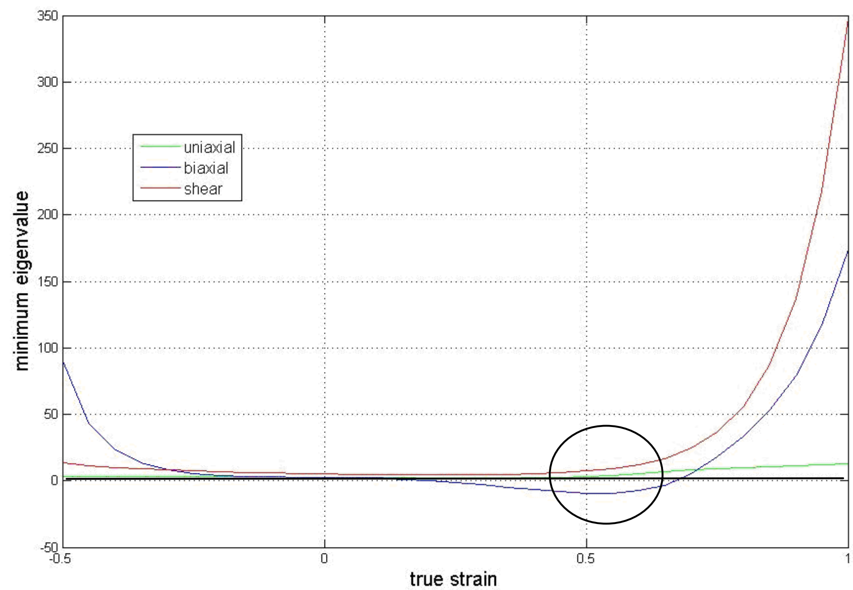

Figure 4.13 Stability curves of a-fit Ogden model

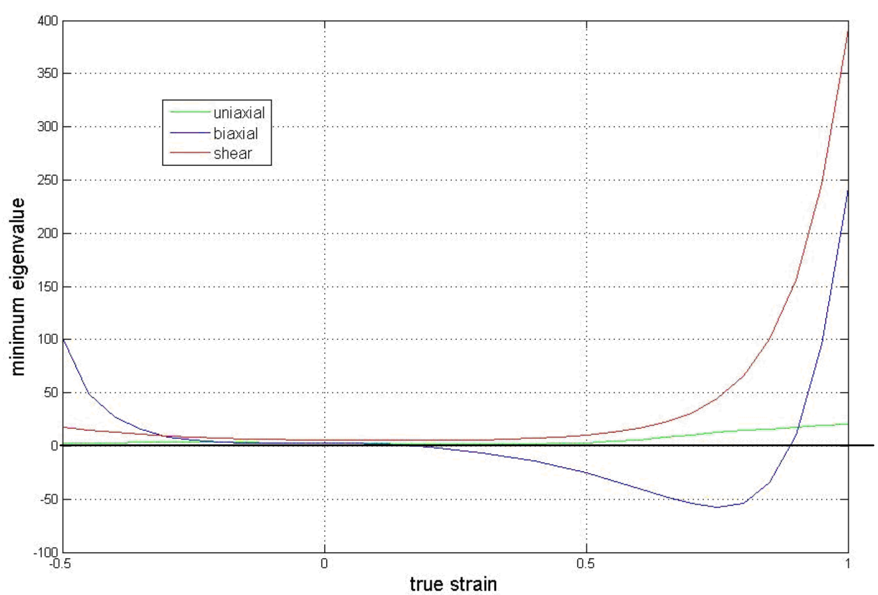

Figure 4.14 Stability curves of b-fit Ogden model

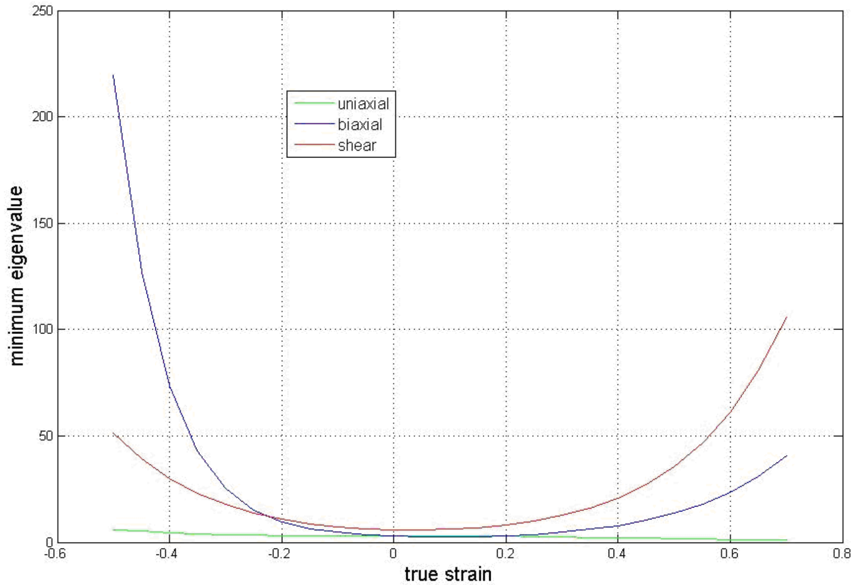

Figure 4.15 Stability curves of c-fit Ogden model

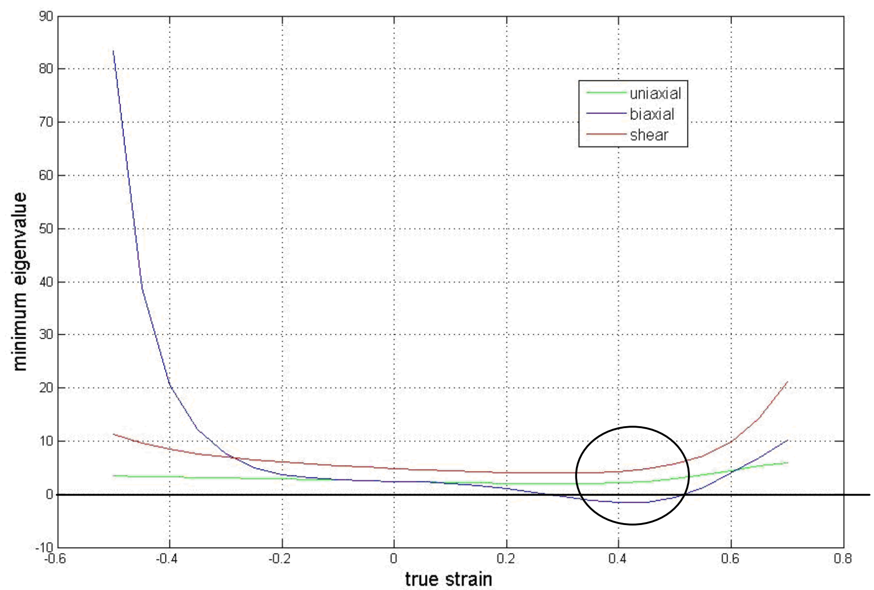

Figure 4.16 Stability curves of e-fit Ogden model

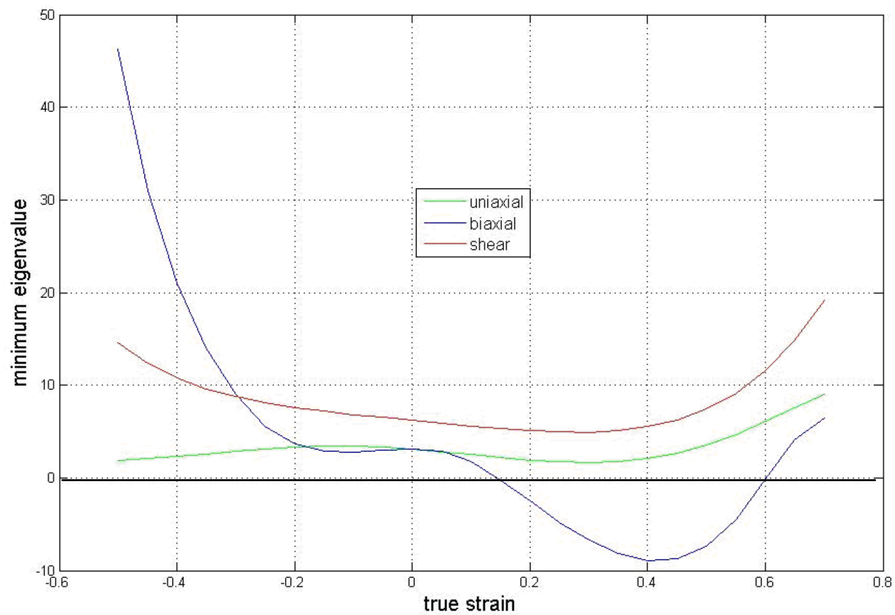

Figure 4.17 Stability curves of Ogden model directly built in ADINA

However it can not be concluded that αs of Ogden model should all be positive because in fact the αs of ADINA-fit Ogden model are also all positive but the model is not always stable. By careful examination of the values of αs and μs, it is observed that, in these simulation results, if the products of each pair of α and μ are positive, then the material was stable. For the ADINA-fit Ogden model, although all αs are positive, there is a negative μ, which makes the material unstable in biaxial deformation. On the other hand, all αs and μs of c-fit Ogden model are positive, and correspondingly the c-fit Ogden material is always stable.

(4) Arruda-Boyce model using P.A.J. van den Bogert and R. de. Borst's data

As observed in chapter 3.2, Arruda-Boyce model produces correct z-displacement during the non-homogenous deformation. Correspondingly all the stability curves of

Arruda-Boyce model are positive as shown in figure 4.18, which makes it always stable.

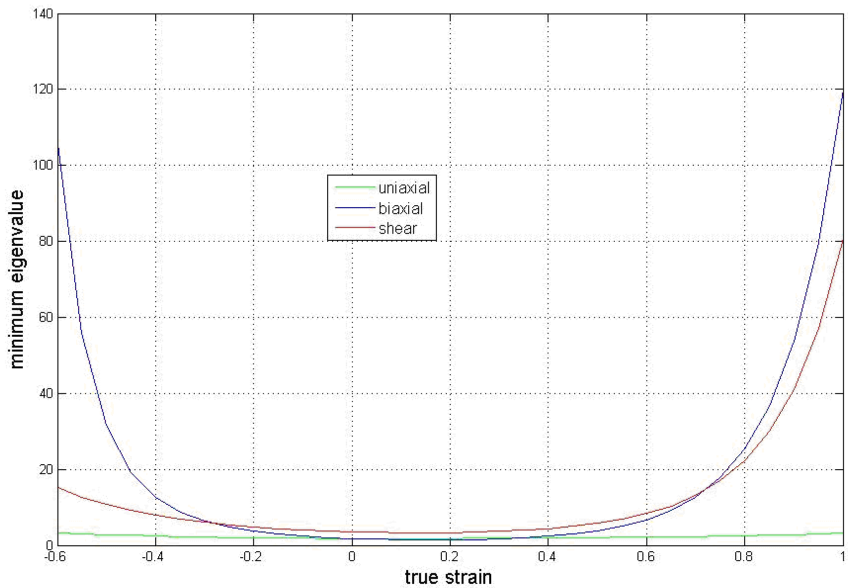

Figure 4.18 Stability curves of Arruda-Boyce model directly built in ADINA

(5) Sussman-Bathe model using P.A.J. van den Bogert and R. de. Borst's data

The stability curves of the three Sussman-Bathe models built in chapter 3.2 are not always positive as shown in figures 4.19, 4.20 and 4.21 and their stability curves are fairly similar to corresponding Ogden models which they are built from. The Sussman-Bathe model which was built from c-fit Ogden model is always stable as shown in figure 4.20. During the simulation carried out in chapter 3.2, it is also the only Sussman-Bathe model which produces correct z-displacement. This implies that the stability of Sussman-Bathe model relies on the uniaxial data from which the Sussman-Bathe model is built.

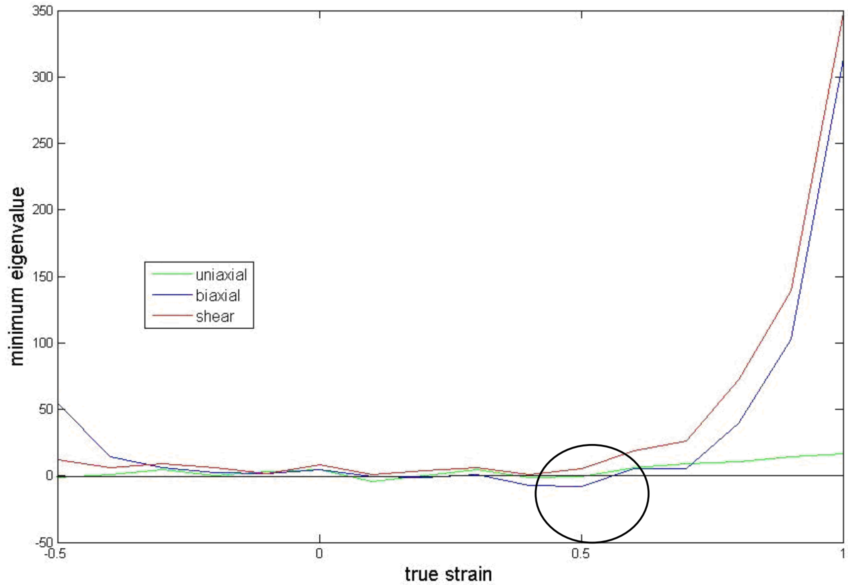

Figure 4.19 Stability curves of Sussman-Bathe model build from a-fit Ogden model

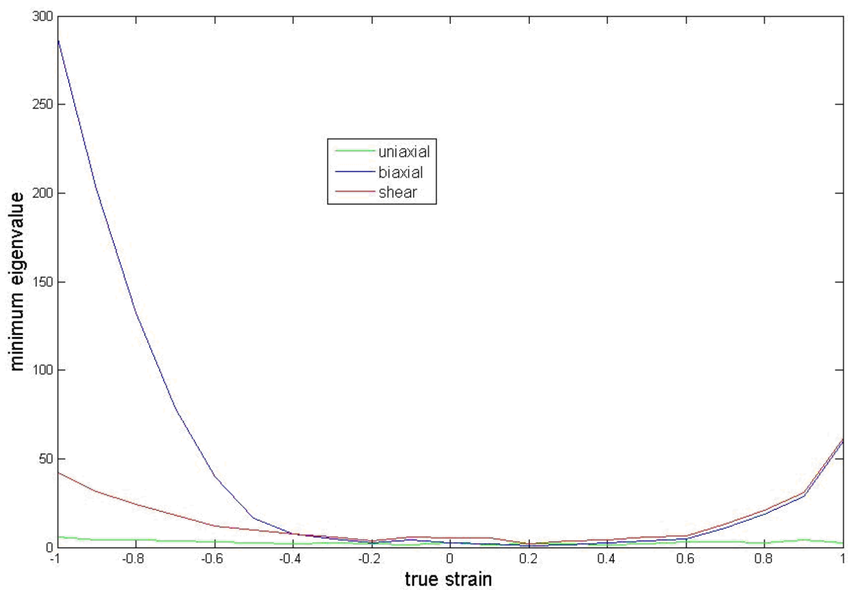

Figure 4.20 Stability curves of Sussman-Bathe model build from c-fit Ogden model

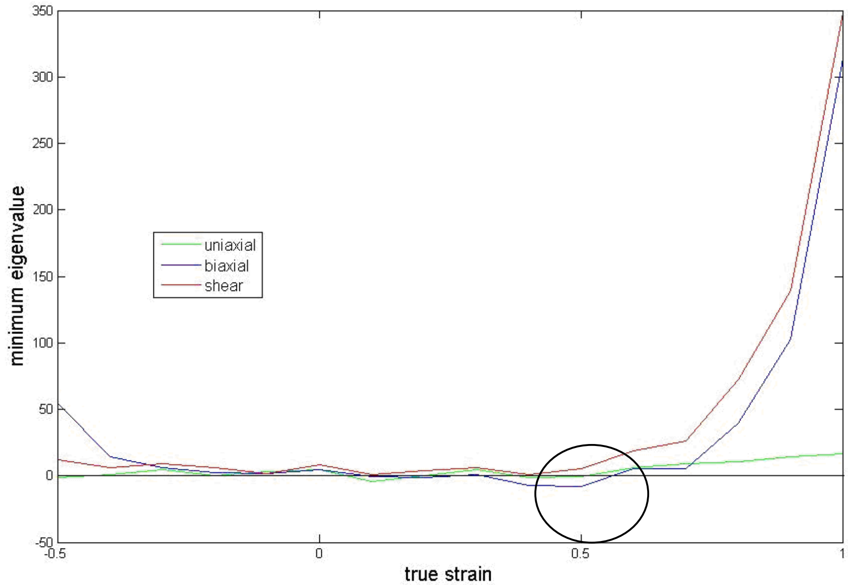

Figure 4.21 Stability curves of Sussman-Bathe model build from ADINA-fit Ogden model

Compared with stability curves of Ogden models in figure 4.13, 4.15 and 4.17, there are wiggles for Sussman-Bathe model. Indeed, there is no smooth function for the Sussman-Bathe model. The Sussman-Bathe model is so close to the experimental data that if there are some uncertainties in the experimental data, it will propagate to the Sussman-Bathe model.

From the stability analysis of rubber material models which are employed in the non-homogenous shear deformation tests in chapter 3.2, it can be concluded that the stability of material models affect their predicative capability greatly. Only when the material model is always stable, a correct simulation result for non-homogenous deformation could be achieved.

Chapter 5

Conclusions

The predictive capability and stability of a rubber material model should be considered jointly to achieve a physically correct numerical simulation result.

The predictive capability, ranging from the uniaxial extension and compression, biaxial deformation, pure shear deformation to more general non-homogenous deformations, is essential for rubber material models. Both extension and compression experimental data are required to build a correct material model. Hence, in this thesis, rubber material models are built with Treloar' s experimental data of compression and extension, and further used to analyze all other forms of deformations, like pure shear and 3-D non-homogenous shear deformations.

The four commonly used rubber material models: Mooney-Rivlin model, Ogden model, Arruda-Boyce model and Sussman-Bathe model are analyzed theoretically and tested numerically. Among these four rubber material models, only the Sussman-Bathe model can fit both extension and compression experimental data perfectly while for the other three models, there are significant departures from the experimental data, which is even more evident for the compression experimental data.

Regarding the predictive capability of rubber material models, only the Sussman-Bathe model predicts a perfect pure shear deformation stress-strain curve which coincides with the experimental data. Both the Ogden model and Arruda-Boyce model produce slightly higher curves while the result from the Mooney-Rivlin model departs significantly. Furthermore, a non-homogenous shear deformation simulation with the various rubber material models was carried out and the results show that Arruda-Boyce model, Ogden model with certain constraint toward its parameters, and Sussman-Bathe model could produce correct simulation results.

The stability of the rubber material models can affect their predictive capability greatly. Therefore, the newly available stability criterion in ADINA is re-derived and numerically verified through simulation tests in ADINA. If the material model is not stable, its corresponding parameters must be adjusted to achieve correct simulation results.

The stability of all three major deformations is required to ensure a correct non-homogenous deformation. The stability of Mooney-Rivlin model is not good and it seems to be impossible to stabilize all three major deformations at the same time, no matter how the model constants are adjusted. For the Ogden model, the stability depends on the characteristics of its parameters. If all the products of α and μ are positive, then the Ogden model will be stable. However this is only a sufficient requirement and sometimes even when the products are not all positive, the Ogden model is still stable by numerical test results. Hence, the development of a sufficient and necessary condition to have a stable Ogden model is suggested for future study. Arruda-Boyce model has good stability because of its physical background. The stability of Sussman-Bathe model is greatly influenced by the uniaxial experimental data which the model is built on.

The Sussman-Bathe model is so close to the experimental data that any noise in experimental data will cause oscillation in the Sussman-Bathe model. Furthermore, due to the characteristics of cubic spline curve-fitting, which is employed in the Sussman-Bathe model, wiggles in stress-strain curves and stability curves may appear. Therefore, a smoothing algorithm is suggested to be included into the Sussman-Bathe model in future studies.

Bibliography

[1] K.J. Bathe, *Finite Element Procedures*, Prentice Hall, (1996).

[2] Z.Y. Guo, X.Q. Peng and B. Moran. A composites-based hyperelastic constitutive model for soft tissue with application to the human annulus fibrosus, *Journal of the Mechanics and Physics of Solids*, 54(9), pp 1952-1971 (2006).

[3] E.S. Almeida, R.L. Spilker, Finite element formulations for hyperelastic transversely isotropic biphasic soft tissues, *Computer Methods in Applied Mechanics and Engineering*, Volume 151, Issues 3.4, pp 513-538, 20 January (1998).

[4] M. Mooney, A theory of large elastic deformation, *J. Appl. Physics*, 2, pp 582-592 (1940).

[5] R.S. Rivlin, Large elastic deformations of isotropic materials. IV. Further developments of the general theory, *Philos. Trans. Roy. Soc*. A 241, pp 379-397 (1948).

[6] R.W. Ogden, Large deformation isotropic elasticity-on the correlation of theory and experiment for incompressible rubber-like solids, *Proc. Roy. Soc*. A 326, pp 565-584 (1972).

[7] E. Arruda, and M. Boyce, A three-dimensional constitutive model for the large stretch behavior of rubber elastic materials. *J. Mech. Phys. Solids*, 41, pp 389-412 (1993).

[8] T. Sussman and K.J. Bathe, A model of incompressible isotropic hyperelastic material behavior using spline interpolations of tension-compression test data, *Communications in Numerical Methods in Engineering*. Available on line: *http://www3.interscience.wiley.com/cgi-bin/fulltext/117905580/PDFSTART*

[9] E. Arruda, and M. Boyce, M. Constitutive models of rubber elasticity: a review, *Rubber Chemistry and Technology*, 73(3), pp 504-523, (2000).

[10] P.A.J. van den Bogert and R. de. Borst, On the behaviour of rubber-like materials in compression and shear, *Archive of Applied Mechanics*; 64, pp 136-146, (1994).

[11] P.A. Przybylo, and E. Arruda, Experimental investigations and numerical modelling of incompressible elastomers during Non-Homogeneous Deformations, *Rubber Chemistry and Technology*, Vol. 71, No. 4, pp 730-749, (1998).

[12] R.S. Rivlin, Some thoughts on material stability, *Finite Elasticity*, Martinus-Nijhoff Publishers, London, pp 105-199, (1982).

[13] K.I. Romanov, The Drucker stability of a material, *Journal of Applied Mathematics and Mechanics*, 65 (1), pp 155-162, (2001).

[14] K.J. Bathe, private communications with author, (2008).

[15] J.M. Ball, Constitutive inequalities and existence theorems in nonlinear elastostatics, *Nonlinear Analysis and Mechanics: Heriot.Watt Symposium*, volume 1, pp187-241, (1977).

[16] J.M. Ball, Convexity conditions and existence theorems in nonlinear elasticity, *Archives for Rational Mechanics and Analysis*, 63, pp 337-402, (1977).

[17] Y. Obata, S. Kawabata, and H.Kawai. Mechanical properties of natural rubber vulcanizates in finite formation, *Journal of Polymer Science*, Series A.2, 8, pp 903-919, (1970).

[18] K.C. Valanis, R.F. Landel, The strain-energy function of a hyperelastic material in terms of the extension ratios, *J. Appl. Physics*, 38(7), pp 2997-3002, (1967).

[19] L.R.G. Treloar, *The Physics of Rubber Elasticity*, Oxford University Press, 1975

[20] F. T. Wall, Statistical thermodynamics of rubber. II, *J. Chem. Phys*. 10, pp 485, (1942).

[21] L.R.G. Treloar, Stress-strain data for vulcanised rubber under various types of deformation. *Trans. Faraday Soc.* 40, pp 59-70, (1944).

[22] M.C. Wang and E. Guth, Statistical theory of networks of non-gaussian flexible chains, *J. Chem. Phys.* 20, pp 1144 (1952).

[23] P. J. Flory and J. Rehner, Jr., Statistical mechanics of cross-linked polymer networks I. rubberlike elasticity, *J. Chem. Phys.* 11, pp 512 (1943).

[24] L.R.G. Treloar, The elasticity of a network of long-chain molecules. III. *Trans. Faraday Soc.*, 42, pp 83-94. (1946)

[25] P.D. Wu and E. van der Giessen, On improved network models for rubber elasticity and their applications to orientation hardening in glassy polymers, *Journal of the Mechanics and Physics of Solids*, 41, pp 427-456 (1993).

[26] H. Lobo and T. Bethard, Practical issues in the development and implementation of hyperelastic models, Datapoint Testing Services, online documents.

[27] L.R.G. Treloar, *The Physics of Rubber Elasticity*, Oxford University Press, pp 245, (1975).

[28] J. Bonet and R.D. Wood. *Nonlinear Continuum Mechanics for Finite Element Analysis*, Cambridge university press, Cambridge, UK, (1997).

[29] *ADINA Structures -Theory and Modeling Guide*, 3.8, pp 339-341, (2008).

[30] L.R.G. Treloar, Stress-strain data for vulcanised rubber under various types of deformation, *Transactions of the Faraday Society*, Vol.40. pp 59-70, (1944).

[31] T Sussman, K.J. Bathe, A finite element formulation for nonlinear incompressible elastic and inelastic analysis, *J. Computers & Structures*; 26, pp 357-409, (1987).

[32] *ADINA Theory and Modeling Guide*, ARD 08.7, Feb, (2008).

[33] *ADINA AUI Primer*, ARD 08.6, Feb, (2008).

[34] R.W. Ogden, *Non-Linear Elastic Deformations*, Ellis Horwood Limited, (1984).

[35] P.A.J. van den Bogert, *Computational Modeling of Rubberlike Materials*, PhD thesis, TU Delft (1991).